



TALLINN UNIVERSITY OF TECHNOLOGY

SCHOOL OF ENGINEERING

Department of Electrical Power Engineering and Mechatronics

MODELLING AND SIMULATION OF A POWER TRANSFORMER USING NUMERICAL THERMAL ANALYSIS

TOITETRAFO MODELLEERIMINE JA SIMULEERIMINE, KASUTADES ARVULIST SOOJUSANALÜÜSI

MASTER THESIS

Üliõpilane: Jaewook Chung

/nimi/

Üliõpilaskood: A165591

Juhendaja: Dmitri Nešumajev, Senior Researcher

/nimi, amet/

Tallinn 2019

(On the reverse side of title page)

AUTHOR'S DECLARATION

Hereby I declare, that I have written this thesis independently.
No academic degree has been applied for based on this material. All works, major viewpoints and data of the other authors used in this thesis have been referenced.

"..03..."January..... 2020...

Author: Jaewook Chung

/signature /

The thesis is in accordance with terms and requirements

"...03..." ...January..... 2020....

Supervisor: ... Dmitri Nešumajev

/signature/

Accepted for defence

".....".....20... .

Chairman of theses defence commission:

/name and signature/

Non-exclusive Licence for Publication and Reproduction of Graduation thesis¹

I, Jaewook Chung (name of the author) (date of birth: 25.03.1970)
hereby

1. grant Tallinn University of Technology (TalTech) a non-exclusive license for my thesis

Modeling and Simulation of a Power Transformer using Numerical Thermal Analysis,

(title of the graduation thesis)

supervised by Dmitri Nešumajev,

(Supervisor's name)

1.1 reproduced for the purposes of preservation and electronic publication, incl. to be entered in the digital collection of TalTech library until expiry of the term of copyright;

1.2 published via the web of TalTech, incl. to be entered in the digital collection of TalTech library until expiry of the term of copyright.

1.3 I am aware that the author also retains the rights specified in clause 1 of this license.

2. I confirm that granting the non-exclusive license does not infringe third persons' intellectual property rights, the rights arising from the Personal Data Protection Act or rights arising from other legislation.

¹ *Non-exclusive Licence for Publication and Reproduction of Graduation Thesis is not valid during the validity period of restriction on access, except the university's right to reproduce the thesis only for preservation purposes.*

_____ *(signature)*

03.January 2020 *(date)*

THESIS TASK

Student:Jaewook Chung.....A165591.....(name, student code)

Study programme, ...MAHM.....Mechatronics..... (code and title)

main speciality:

Supervisor(s): Senior Research Scientist, Dmitri Nešumajev (T.620-3910)

Consultants:(name, position)

..... (company, phone, e-mail)

Thesis topic:

(in English) MODELLING AND SIMULATION OF A POWER TRANSFORMER USING NUMERICAL THERMAL ANALYSIS

(in Estonian) ...TOITETRAFO MODELLEERIMINE JA SIMULEERIMINE, KASUTADES ARVULIST SOOJUSANALÜÜSI...

Thesis main objectives:

1. To study the theory of 3 phase transformer and heat transfer
2. To create a 3D numerical thermal model of a power transformer
3. To analyze and compare the results of the simulation and the experiment

Thesis tasks and time schedule:

No	Task description	Deadline
1	Literature review on the power transformer and thermal analysis	15.Oct. 2019
2	The building of the detailed model in Comsol Multiphysics	31.Oct. 2019
3	A lab experiment on the model and analysis	15.Nov. 2019
4	Computer simulation and comparison with the experiment	10.Dec.2019
5	Compilation and elaboration on the thesis	24.Dec. 2019

Language: English **Deadline for submission of thesis:** "...03..."January 2020....a

Student:Jaewook Chung..... "...03..."January.....20.....a
/signature/

Supervisor: ...Dmitri Nešumajev..... "...03..."January.....20.....a
/signature/

Consultant: "...03..."January.....20.....a
/signature/

Head of study programme: "...03..."January.....20.....a
/signature/

Terms of thesis closed defence and/or restricted access conditions to be formulated on the reverse side

CONTENTS

List of abbreviations and symbols	2
INTRODUCTION.....	3
1. LITERATURE REVIEW	5
1.1 Iron losses	5
1.2 Thermal analysis	6
2. POWER TRANSFORMER.....	9
2.1 Steel core transformer	10
2.2 Three-phase Delta-Star system.....	11
2.3 Transformer losses	14
2.3.1 Total power losses and ΔB	15
2.3.2 Copper losses	15
2.3.3 Iron losses	16
3. HEAT TRANSFER	19
3.1 Conduction	20
3.2 Convection	21
3.3 Radiation.....	23
4. LAB EXPERIMENT.....	25
4.1 No-load test (Open circuit test)	25
4.2 Short circuit test (Impedance test)	27
4.3 Load test and temperature measurement	28
4.3.1 Uncertainty	30
4.3.2 Experiment results	30
5. Heat Transfer Model	35
5.1 Geometry and material property	35
5.2 Boundary conditions	36
5.3 Heat sources and air domain.....	38
5.4 Anisotropic heat transfer in the E-Core.....	40
5.5 Meshing	41
6. Simulation result	48
6.1 Temperature analysis.....	49
6.2 Heat flux analysis.....	52
6.3 Airflow analysis.....	57
6.4 Conclusion and discussion	61
SUMMARY.....	64
LIST OF REFERENCES	65
APPENDICES	67

List of abbreviations and symbols

AC: Alternating current

B : Magnetic flux density (Wb/m² or Tesla),

CEMF: Counter electromotive force

CFD: Computational fluid dynamics

DC: Direct current

FEM: Finite element method

Gr: Grashof number

HV: High voltage

IR: Infrared

H : Magnetic field intensity (H)

h : heat transfer coefficient (W/m²•K)

k : Thermal conductivity (W/ m•K)

LV: Low voltage

I_L : Line current (A)

I_P : Phase current (A)

NU : Nusselt number

P_{Cu} : Copper losses or resistive losses (W)

P_{Fe} : Iron losses or core losses (W)

Pr: Prandtl number

Ra: Rayleigh number

RANS: Reynolds averaged Navier-Stokes equations

V_L : Line voltage (V)

V_P : Phase voltage (V)

INTRODUCTION

Ever since the electronic devices have become a crucial part of the industry, the heat problem has come hand in hand. Joule heating, inductive heating and microwave heating according to the operating power and frequency are of significant factors not to be overlooked when designing and operating electrical machines.

A power transformer, an essential device to reduce or boost voltage, also generates heat during its operation caused by joule losses (resistive losses or copper losses) and iron losses (hysteresis and eddy currents).

The thesis is to implement the numerical modelling and simulation of thermal behaviour of a three-phase transformer using Comsol Multiphysics and experimental values for heat sources. Then the discussion on some of the important factors and correlations between temperature and heat flux will follow.

As can be seen in 1. LITERATURE REVIEW, a lot of studies on thermal analysis of power transformer are performed on heavy-duty industrial transformers with the oil-immersed cooling system. Heavy-duty transformers are definitely more susceptible to heat requiring more active cooling system such as oil and forced convection.

However, the thermal aspect should also be considered in designing and modelling of small or medium-duty air-cooled power transformers because excessive heat impacts on the durability and the performance of the device as much as the heavy-duty ones. For this purpose, light-weighted simulation can be modelled using simple but powerful CFD tools. Identifying the heat transfer mechanism and the temperature distribution can improve the longevity of the device by applying proper insulating or heat-dissipating materials. It could also help to redesign or modify the geometry of the device. All these can be implemented by modelling and simulation in the computer before building an actual prototype.

Comsol Multiphysics is a software that combines FEM analysis and multiphysics simulation. It is widely used to build and simulate models based on complicated partial differential equations in electrical, mechanical, and chemical engineering. Comsol Multiphysics 5.4 is to be used to study and simulate the thermal behaviour of the transformer. To simplify the model, both isotropic and anisotropic heat transfer coefficients are studied and applied according to the material characteristics. The heat generated by the copper windings is derived mathematically first so that the Comsol

Multiphysics handles the heat transfer process over the entire device as well as to the air. Analytical results gained from the simulation are discussed and compared with the experimental data.

The goal of the study is to establish a light-weighted but efficient thermal model of a power transformer which complies with the real-world heat transfer physics.

Therefore, to validate the simulation and obtain exact values for heat sources, a lab experiment to measure the overall surface temperature of the actual model transformer is performed as well. Further analysis, comparison and discussion based on the experiment and the post-processed data are presented.

1. LITERATURE REVIEW

Literature review for this study is carried on 2 areas. One is for iron losses and the other for thermal analysis and heat transfer model of transformers. Study models of the losses are significant because they act as heat sources of the model in this study and thermal analysis is the ultimate goal of the research.

Copper losses are relatively straight forward compared with iron losses. A simple mathematical model can be applied to calculate the copper losses as presented in 2.3.2 Copper losses, whereas deriving iron losses requires much more complicated processes and different approaches.

1.1 Iron losses

Unlike copper losses, calculating iron losses is not simple. It is mainly due to the nature of ferromagnetic materials that involves many heterogeneous parameters while inducing magnetic flux. Many kinds of research have performed but they all require validation with the experimental results. It is stated by [1] that change in magnetization tends to happen in a local domain which is also subject to movement in an irregular pattern. This results in non-uniform magnetization in ferromagnetic material which makes it hard to calculate the exact iron losses analytically or mathematically.

Regarding the iron losses, a lot of researches are carried out based on a widely used power equation by Steinmetz model [2]. However, to find out the Steinmetz coefficients, one must know full detailed information of the core geometry such as exact values of the sheet metal thickness and the width of the sheet surface crossed by the magnetic flow [3]. The study [3] was carried based on a simplified electrical diagram for a single-phase transformer. However, experiments have to be carried out to obtain and verify the B-H characteristic of the transformer. The analytical calculations were acceptable to obtain eddy current loss, but not hysteresis loss.

The study [4] uses two models (Steinmetz equation and the improved generalized Steinmetz equation) and couples them with Comsol Multiphysics. To deal with inhomogeneity in magnetic flux density distribution, separate FEM model is made and non-linearity is handled by defining an initial magnetization curve in Comsol material properties. Post-processing has to be followed to finally obtained the maximum magnetic flux density. For the material, values of Steinmetz constants k , a , b were

obtained according to the frequency and maximum B . Although the numerical results demonstrate good accuracy, it requires multiple time-dependent simulations to achieve empirical current waveforms and still needs validation with experimental results.

A similar approach was carried in the study [5] to achieve loss density using Comsol Livelink with Matlab based on Bertottis equation [6] for heavy-duty hydro generator. FEM program is used to model the losses in the element-level and sum up at the last. Nevertheless, the method seems limited to find the peak AC flux density for this study.

The main goal of the study is to establish a viable heat transfer model of a power transformer and verify with the real temperature under fully loaded operation condition. Therefore, taking exact values of copper losses and iron losses from the experiment is adopted in this study.

1.2 Thermal analysis

In order to perform and establish thorough modelling of heat transfer for a dry-type transformer, review on the preceding studies is summarized as follows.

A slice model of an oil-filled air cooling transformer was studied by J. Gastelurrutia [7]. The study was focused on the heat transfer mechanism and the oil flow especially on a hallow fin of the transformer. Making a model into a slice could save computational resources and time considerably. Also, measurement on the surface temperatures of 3 similar but different types of transformers with different loads were performed to verify the robustness of the slice model.

The study demonstrated viability when focusing the heat transfer associated with the oil flow inside the hallow fins. Although turbulence was modelled and it conveyed the entire thermal behaviour of the transformer, the dynamics of the heat transfer, especially inside the transformer case, was not in the study scope. Thermocouples to measure the temperatures were attached on the case surface and the hollow fins, not on the internal surfaces.

Additionally, because of the model being sliced, the slice model showed a higher temperature than the complete model, and loss values of the core and the windings

were taken from the loading guide for oil-immersed power transformer. A mean value of the heat transfer coefficient was set for the fins surfaces without assigning the air domain. This could have resulted in a considerable difference in temperature vertically especially on the lower part of the model as was commented on the paper as well. The study was carried out under the assumption that no radiation in the air.

Torriano [8] carried a numerical study on an oil-immersed disc type transformer modelled in 2D conjugate heat transfer (CHT) which couples solid models and the fluid model. Heat source data is presumed to be gained from the manufacturer or the operator and Navier-Stokes equations for incompressible flow is applied for governing equations. The study deals not only with heat transfer but also the oil flow momentum and viscosity. The oil flow is considered as laminar and no turbulence is modelled. It's a parametric study to analyze the effect of mass flow rate, inlet position, and inlet temperature profile of the oil that flows around the winding.

The study focused on the failure of the device due to a thermal impact was done by Pelayo [9] using a 2D model cut in the middle so that the cross-section of the windings are viewed. A microscopic modelling in the copper windings including air was implemented in the study, however, radiation was not considered and turbulence was not modelled. The process to derive iron losses was missing discussing only the copper losses. In general, the study focused on the overload condition due to a failure of the winding insulation.

By El Wakil [10], a numerical study on the cooling optimization of a power transformer was carried in 6 different geometric configurations and the cooling oil flow rates under the steady-state. The work was done by giving increment of inlet fluid velocities while keeping the oil temperature constant. The influence of the parameters (inlet velocities and different geometries) on the fluid flow and the heat transfer was analysed. Finally, the geometric parameters were changed by adding or removing insulation materials on the top, bottom, channels core, and windings. It was concluded with the selection of the best geometry case and proposing the optimum inlet velocity.

Lee [11] studied the air temperature effect on a transformer placed in a vertical cooling duct. The 2D model was created to simulate transient heat diffusion of a transformer to study how the air temperature in the duct affects the winding temperature. The study attempted to couple electromagnetic and thermal models together. As for the heat sources, the current density is used in the governing equations for both copper losses and iron losses. However, it was not clearly

mentioned how exact values of source currents were achieved. So it could be assumed that the values should have achieved somehow from the experiments. The temperature distribution is calculated with constant and varying air temperatures under different loads.

As can be reviewed from the above, most of the researches were carried out based on the oil-immersed transformers and in the 2D model. Transformer using oil as a cooling medium has to deal with the fluid flow together making models more complicated solving for the fluid dynamic problem, thus making it really hard to model in 3D.

Additionally, most of the researches missed out the details on how the heat sources were obtained whether numerically or experimentally. The exact values of heat sources are crucial initial conditions since everything starts from there. One mentioned in detail was not engaged with thermal analysis.

The goal of this study is to achieve a whole 3D model of a dry-type power transformer that complies with the experimental results and provide sufficient information of heat flux and temperature information. Therefore, it would be meaningful to perform a study on a 3D axisymmetric model of a transformer without oil and fins and analyse heat fluxes and temperatures inside and the surface of the device.

2. POWER TRANSFORMER

A transformer is a power electronic device to elevate or descend the AC voltage to the desired output voltage using mutual inductance. The key principle of the device is based on Michael Faraday's law of induction which defines the production of a magnetic field when current flows [12]. It transfers energy and regulates the voltage simultaneously using this common magnetic field generated along with the steel core. Transformer plays a crucial role in power electric transmission and distribution system since high voltage is more efficient to transport the electrical energy over a long distance with minimal losses [12]. Higher the voltage is, the lower the I^2R losses are. After the power transmission, the high voltage electricity can be lowered to a safer voltage(220 V or 110 V) for the end-users and transformers take crucial roles in this process.

Modern power transformer, which has an efficiency between 95% and 99%, requires little maintenance and adjustment for operation due to its simple construction and static operation [12]. Nevertheless, like all other electric devices, heat is generated by the power transformer when a load is applied during the operation. Thermal analysis of a power transformer is required in order to predict the surface temperature distribution as well as to analyze how heat is transferred by all modes of heat transfer. These results could possibly prevent the overheating of the device by applying proper thermal materials or design a natural or forced cooling system on the device.

There are two types of power transformer in terms of cooling and insulation type. One is dry type and the other is oil-immersed type. The dry type is air-cooled suitable for small and medium in power and size. Oil-immersed type is widely used in the industry as heavy-duty transformers. Oil is a good conductor of heat but a bad conductor of electricity at the same time. This property of oil makes it possible to use oil as an insulator and a coolant of the heavy-duty transformer in high voltage. Mineral or vegetable oil is commonly used in the oil-immersed industrial transformer.

There are many different types of transformers in terms of usage and function, however, the study is carried out based on a 3 phase dry type transformer(Star-Delta for step up and Delta-Star for step down) shown in Figure 2.1, so the discussion and topic will remain within this specific model.



Figure 2.1 The real model of 3 phase power transformer (0,5 KVA; 380 V/110 V)

The measured geometry of the model transformer is listed in Table 2.1, and more detailed electrical technical specifications are presented in the following sections and chapter 4.

Table 2.1 Measured geometry of the transformer

E-core	width	150 mm
	height	152 mm
	depth	40 mm
Single copper winding	width	52 mm
	height	60 mm
	depth	85 mm

2.1 Steel core transformer

The core made of steel carries magnetic flux when current flows through copper wires. The core material is magnetic so that it carries magnetic flux much better than other media as air and it is widely available in the industry. For example, electrical steel has relative permeability (μ_r), referred to as an ability to carry flux, around 1500 while air has a value of 1.

Magnetic flux can be defined as follows.

$$B = \mu_o \cdot \mu_r \cdot H \quad (2.1)$$

Where B is the magnetic flux density (Wb/m² or Tesla),

μ_o is the free space permeability = $4\pi \cdot 10^{-7} \text{ Wb} \cdot \text{A}^{-1} \cdot \text{m}^{-1}$

μ_r is the relative permeability of the material

H is the magnetic field intensity (H)

It must be noted that the relationship between B and H is expressed in the B - H curve as the value of μ_r changes with flux. Since a transformer is a device to transfer electrical energy through magnetic flux, concentrating the flux definitely improves the efficiency of the transformer [12].

Note that B and H can be rewritten and be represented in terms of flux [13].

$$B = \frac{\phi}{A} \text{ and } H = \frac{I \cdot N}{d} \quad (2.2)$$

where ϕ is the core flux lines (Wb),

A is the cross-sectional area of the core (m^2),

N is the number of turns in the winding,

I is the maximum current (A),

d is the mean length of the coil (m).

Rearranging (2.1) and (2.2) with the frequency, we obtain an expression of flux density(B) useful for transformer design [13] as follows

$$B = \frac{\phi}{A} = \frac{0,225 \times E}{f \cdot A \cdot N} \quad (2.3)$$

where E is the applied alternating voltage (V)

f is the frequency (Hz)

2.2 Three-phase Delta-Star system

A three-phase transformer is typically used to regulate the voltage of the 3-phase power supply. A three-phase transformer is equivalent to three sets of single-phase transformers sharing a common core.

There are only 2 ways to connect 3 wires in 3 phase power system. One is Delta and the other is Star(Wye). In Delta configuration, 3 transformers end-to-end are connected in series, whereas in Star configuration, there is one point which is the neutral shared by 3 wires whose physical wirings are shown in Figure 2.2.

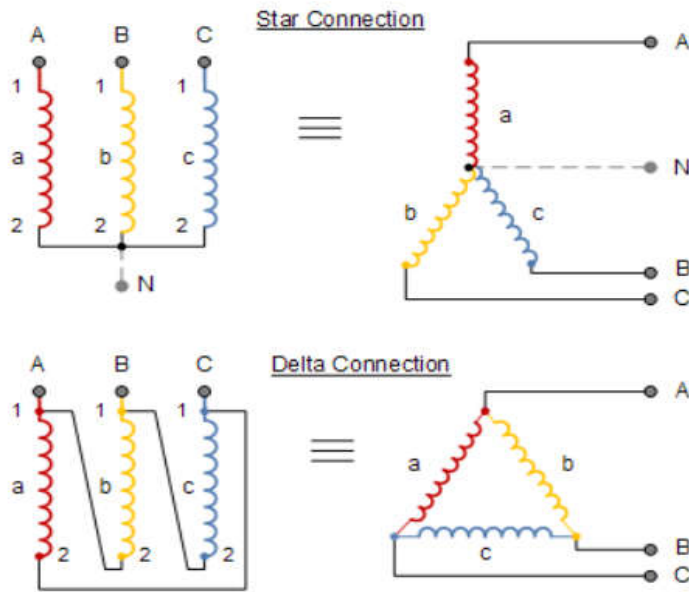


Figure 2.2 Physical wiring of star and Delta connection [14]

In Delta system, the voltage between any 2 line voltages must be identical to the coil voltage that is referred as the phase voltage since they are connected with the coil in parallel, resulting $V_L = V_p$. However, the relationship between the line current and the phase current is 120° out of phase, resulting $I_L = I_p \times \sqrt{3}$ [12].

In the Star system, the difference in phase-time by 120° happens in the voltage between 2 line conductors resulting $V_L = V_p \times \sqrt{3}$. As for the current, there is only one path for the current to flow through the load connected between 2 line conductors giving $I_L = I_p$. If one more extra line is connected to the common point called a neutral, four-wire system can be formed in 3 phase system making it possible to create one more voltage to supply the loads. It makes the star system most popular in 3-phase system[12] in the industry.

The total KVA of the 3-phase system is the sum of each individual phase coil. Providing that all have equal power, the total 3-phase power can be represented as follows [12].

$$\text{Three phase KVA} = \frac{3 \times V_p \times I_p}{1000} \quad (2.4)$$

However, the actual calculation of KVA differs according to how 3 phase power system is connected in the circuit. There can be a total of 4 different options based on how circuits of primary and secondary windings are wired.

- Star-Star (Wye-Wye)

- Star-Delta (Wye-Delta)
- Delta-Star (Delta-Wye)
- Delta-Delta

In general, Delta connection offers chances for multiple voltages but Delta connection provides higher reliability [15]. Phase shift takes place from primary to secondary in the Delta-Star transformer, whereas no phase shift is involved in Delta-Delta or Wye-Wye type transformers.

As a Delta-Star(Star-Delta) connection transformer is chosen for this study, the discussion will stay within this type in this paper. The circuit diagram of the Delta-Star connection transformer is shown below.

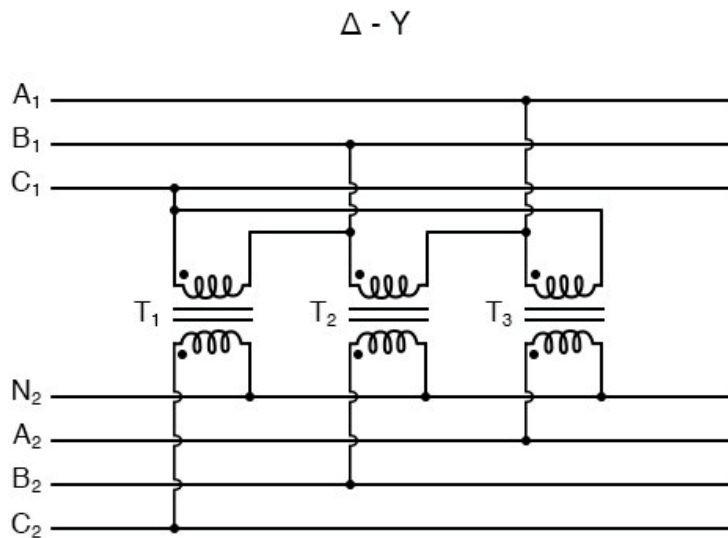


Figure 2.3 Phase wiring of Delta-Star transformer [15]

This type of transformer is mainly used when more than one voltage is required on the secondary side depending on the purpose. It is also common to apply this type to a step-up transformer before the transmission of electric power [12]. The main advantage of the Delta-Star type transformer is the extra gain in voltage. Even if the turn ratio between the primary and the secondary is equal, the secondary winding still has 1,73 times higher voltage than the primary side due to the structure of Wye-connection. This is certainly a benefit when the transformer is used as a step-up device [12].

$$\text{Line current} = \text{phase current} \times 1,73 \quad (2.5)$$

Nevertheless, the disadvantages of this type would be

- The primary windings must be insulated throughout the entire 3-phase voltage for a step-down transformer, which requires more insulation materials.
- The secondary Delta-connection does not cancel out harmonic currents.

In the Delta system, $V_p = V_L$ and $I_L = I_p \times \sqrt{3}$ and substituting these into (2.4), will result

$$KVA = V_L \times I_L \times \frac{\sqrt{3}}{1000} \quad (2.6)$$

Turn ratio of 3 phase transformer for Delta-Star connection is defined as

$$TR = \frac{N_p}{N_s} = \sqrt{3} \cdot \frac{V_p}{V_s} \quad (2.7)$$

where N_p is the number of turns of the primary winding,

N_s is the number of turns of the secondary winding,

V_p is the primary winding voltage, and

V_s is the secondary winding voltage.

2.3 Transformer losses

Like all mechanical and electrical devices, a power transformer also encounters considerable losses mainly in a form of heat while transferring energy into different voltages. There are more minor losses involved in the transformer, however, only the major losses directly related to thermal losses are discussed hereunder.

IEEE standards are to measure kVA ratings under an average winding temperature of 55 °C and a hottest-spot temperature of 70 °C. IEEE design limit of maximum temperature is 80 °C, and it is known that for every 6 to 8 °C beyond the limit temperature, the insulation life would decrease by a factor of 2 [13].

Copper losses or resistive losses caused by the joule heating contributes the largest part of the thermal losses of the transformer. Copper windings exert heat by Joule heating when current flows through the wire. Copper losses in the windings depend on the number of phases, AC resistance of the phase winding and current. Iron losses, on the other hand, caused by hysteresis and eddy currents in the steel core are depended on the size of the core and the magnetic flux density.

When an alternating current is supplied to the primary windings of the transformer, it generates an alternating magnetic flux in the core by which flow of current is induced in the secondary winding as defined by Faraday's law of electromagnetic induction.

During this process, a considerable amount of losses occur. Iron losses comprise of hysteresis loss, eddy current loss and excess loss. Excess loss is considered minimal, so only hysteresis and eddy loss are considered in this study.

2.3.1 Total power losses and ΔB

The total power loss of a power transformer is the sum of copper losses and iron losses, expressed as $P_{total} = P_{fe} + P_{cu}$. Further details of each loss are discussed in the following sections.

According to [16], it should be aware that there are trade-off relationship between both losses to be considered together with the peak AC flux density(ΔB). In general, ΔB is proportional to the core losses but inversely proportional to the copper losses. Therefore, the optimum value of ΔB has to be chosen to minimize the total loss of the transformer.

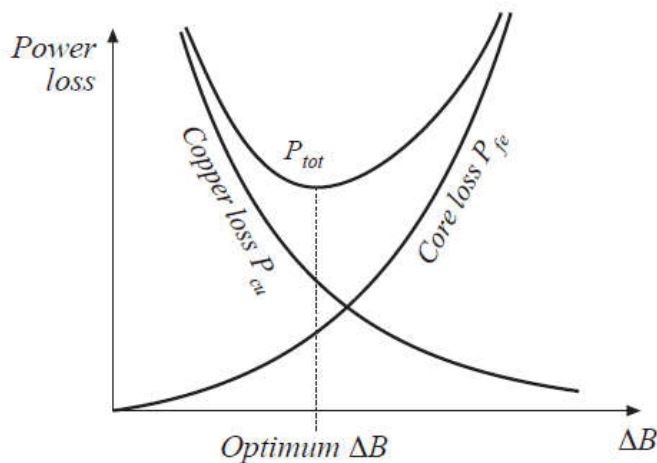


Figure 2.4 Dependency of the total loss on its peak AC flux density [16]

Figure 2.4 illustrates the constraint of setting the ΔB as well as the fact that optimum ΔB does not occur at the cross point of two curves where $P_{cu} = P_{fe}$. It rather appears at the minimum point of the curve P_{tot} where the following equation is satisfied.

$$\frac{dP_{fe}}{d(\Delta B)} = \frac{dP_{cu}}{d(\Delta B)} \quad (2.8)$$

2.3.2 Copper losses

The heat is generated when the current flows through the copper wire and this is called the resistive loss or joule loss. The majority of the heat is generated from the

coil and transferred to other parts by conduction and dissipated to the air by convection and radiation. For thermal analysis, conduction in solids and convection between solid to air as well as radiation are considered.

Mathematical approach[17] can be used to achieve the amount of heat generated by resistive losses (copper losses) from the electrical power source and the CFD tool is to handle only heat transfer simulation.

$$P_{Cu} = \phi I^2 R_{AC} \quad (2.9)$$

where ϕ is the number of phases,

I is the current (A),

R_{AC} is the AC resistance of the phase winding (Ω).

AC resistance of the phase winding is defined as follows.

$$R_{AC} = k_R \frac{N \cdot l_{av}}{\sigma \cdot S_c} \quad (2.10)$$

where k_R is the skin effect factor,

N is the number of turns,

l_{av} is the average length of a turn (m),

S_c is the cross-sectional area of the conductor(m^2), and

σ is the specific conductivity of the copper (S/m).

Since the frequency is 50 Hz (less than 60 Hz) and the wire diameter is less than 1 cm, the skin effect is negligible. All the other parameters can be obtained from the geometry and the material property [17].

2.3.3 Iron losses

Iron losses also known as core losses are generated in ferromagnetic materials when concentrated magnetic flux flows in the material. Iron losses can be further dividend into hysteresis loss and eddy current loss.

Because not all the flux will be transferred to the secondary coil, some flux is lost because of hysteresis which can be described as a tendency of a material to resist rapid changes in magnetic polarity [12]. Hysteresis is caused by the cyclic reversal of

flux in the magnetic circuit. It can be referred to as internal friction of the molecules of the magnetic material [13].

When flux is generated and changes its polarity, a voltage is also induced and make currents to flow in the core. They are called eddy currents and circulate direction normal to the width of the core by the flow of magnetic flux. It can be reduced by the metallurgical control of the steel.

Therefore, laminated steels are designed to have the following properties in order to lower currents and core losses [18].

- High permeability: high B with low H
- High saturation polarization
- Low electrical conductivity to minimize the eddy currents.

Although the heat generated by the iron losses is smaller than that by the copper losses, it is significant enough to consider both for accurate modelling and simulation. Iron losses are generated due to the variations in the flux and they are depended on the magnetic properties of the materials. These losses occur in the transformer core whereas copper losses take place in the coils. Unlike copper losses, iron losses are constant irrespective of the change of the load [17] but rather depended on the voltage and frequency. Eddy current losses are defined as

$$P_{eddy} = k_e (B \cdot f \cdot t)^2 \quad (2.11)$$

where k_e is the eddy current constant,

B is the flux density (T),

f is the frequency(Hz), and

t is the thickness of the material (mm).

Hysteresis loss can be defined as the electrical energy that is required to realign the domains of the ferromagnetic material in the core of the transformer and expressed as

$$P_h = k_h \cdot B^{1.6} \cdot f \quad (2.12)$$

where k_h is the hysteresis constant,

B is the flux density (T) and

f is the frequency (Hz).

As can be seen from equation (2.12) that the losses are depended on the AC flux and the frequency. In general, the no-load loss which is the resistance component of the core loss is usually a guaranteed value that should remain constant as the supply voltage maintains unchanged[13].

Power equation proposed by Steinmetz is an empirical equation to calculate the total iron losses based on the unit volume of the ferromagnetic material. It is assumed that the magnetic flux varies sinusoidally without frequency change[2] resulting

$$P_v(t) = k \cdot f^a \cdot B^b \quad (2.13)$$

Where $P_v(t)$ is the time-average power loss per unit volume (mW/cm³),

f is the frequency,

B is the peak magnetic flux density

K , a , and b are Steinmetz coefficients

Another approach to combine both eddy losses and hysteresis losses is introduced by the approximation in [16] as follows.

$$P_{fe} = K_{fe}(\Delta B)^\beta A_c l_m \quad (2.14)$$

where ΔB is the peak AC flux density

A_c is the cross-sectional area,

l_m is the mean magnetic path length of the core,

K_{fe} is a proportionality constant depends on the frequency, and

β is the ferrite power material factor.

A product of A_c and l_m represents the volume of the core and the value β , provided by the manufacturer, is usually approximately 2,6.

Nevertheless, iron losses can not be directly calculated mathematically due to the unknown constants k_e , k_h , or k_{fe} , which are mostly acquired by the means of experiment. Many studies have presented how to approach to these constants but there is no absolute methodology accurate enough to replace experimental methods. It was one of the reasons why the experiment is performed not only to verify the simulation result but also to obtain the exact amount of iron losses in the specific transformer.

3. HEAT TRANSFER

Heat is defined as a form of energy which is transferrable from one system to another as a result of temperature difference [19]. So when an object is in a position where there is a temperature difference with the surroundings, heat flows from the higher temperature to the lower, and this phenomenon is called heat transfer, heat flow, or heat exchange. Thermal analysis is a study of heat flow conditions and temperature distribution based on such phenomenon and the material properties to be applied to design the insulating or cooling system.

All thermomechanical analysis is based on Energy balance based on the first law of thermodynamics known as the conservation of energy principle [19], which can be expressed as follows.

$$E_{in} - E_{out} = \Delta E_{sys} \quad (3.1)$$

where E_{in} , E_{out} , ΔE_{sys} are energy in, out, and change in energy in the system respectively.

When it comes to surface energy balance where there is no energy rate change because no volume is considered,

$$\dot{E}_{in} = \dot{E}_{out} \quad (3.2)$$

Heat flux can be defined as the rate of heat transfer per unit area normal to the direction of heat transfer, and the average heat flux is expressed as [19]

$$\dot{q} = \frac{\dot{Q}}{A} \quad (W/m^2) \quad (3.3)$$

where \dot{Q} is the amount of heat transfer rate per unit time (W)

A is the heat transfer area (m^2)

It is considered that heat flux changes according to time and the position on a surface.

3.1 Conduction

Conduction can be defined as the transport of thermal energy by intermolecular motion. Heat is transferred even without the bulk movement of the substance. Conduction can happen in solids, liquids, or gases. In fluids, it comes with collisions and diffusion of the molecules in random motion whereas, lattice vibrations of the molecules and the energy transport by free electrons take roles in solids. Since microscopic energy exchange among molecules can not be calculated, Fourier's law governs conductive heat transfer rate in Watt as follows [19].

$$\dot{Q}_{cond} = -k \cdot A \cdot \left(\frac{dT}{dx}\right) \quad (3.4)$$

where k is the thermal conductivity of the material (W/m·K)

dT/dx is the temperature gradient along the distance x , and

A is the area of the heat transfer (m^2).

The temperature gradient, dT/dx , is proportional to the heat conduction rate in a given direction which means the greater the temperature difference, the greater the heat transfer. Thermal conductivity can be referred to as a transport property of the substance to conduct heat and it is not a fixed value but rather variant value according to the molecular structure and intermolecular interactions. For example, the thermal conductivity of pure metals varies between 100 to 400 W/m·K at room temperature but shows the higher value at low temperature. The value of water reaches about 0,7 W/m·K at 200 K but falls as temperature increases [20].

The idea of thermal resistance is a useful concept to understand the phenomena similar to Ohm's law in electrical resistance. Referring temperature as voltage and thermal resistance instead of electrical resistance, a simple steady-state problem can be analyzed. However, in practice, heat transfer by conduction occurs in a multidimensional condition under the following governing equation in the partial differential form [20].

$$\dot{Q} = -kA\nabla T = -k \left[A_x \frac{\partial T}{\partial x} \mathbf{i} + A_y \frac{\partial T}{\partial y} \mathbf{j} + A_z \frac{\partial T}{\partial z} \mathbf{k} \right] \quad (3.5)$$

where ∇ is the vector gradient operator,

k is the thermal conductivity,

A_x, A_y, A_z are heat conduction area normal to x, y, z respectively, and

$[i, j, k]$ are the unit vectors in the Cartesian coordinates.

3.2 Convection

Convection is a heat transfer between a solid face and the adjacent fluid or gas which involve the combined effects of conduction and fluid motion [19]. The fluid will start to flow if there is a change in density caused by the temperature difference. The convection energy transfer refers to the combination of molecular diffusion and bulk fluid motion (advection). The convective heat transfer rate follows Newton's cooling law based on the proportionality between convective heat flow and the temperature difference over the surface area, which can be defined in Watt as follows.

$$\dot{Q}_{convection} = h \cdot A \cdot (T_s - T_f) \quad (3.6)$$

where h is the convective heat transfer coefficient ($W/m^2 \cdot K$),

A is the surface area (m^2),

T_s is the surface temperature, and

T_f is the fluid temperature.

The coefficient h depends on many complex factors such as fluid properties, geometrical configuration, fluid velocity, surface roughness etc [20].

The convective heat transfer coefficient, h , is expressed in terms of nondimensional number called *Nusselt number* (Nu) which represents the temperature gradient at the wall.

$$Nu = \frac{hL}{k} = \frac{(q''/\Delta T)L}{k} \quad (3.7)$$

where h is the convective heat transfer coefficient of the flow,

L is the characteristic length (m), and

k is the thermal conductivity of the fluid ($W/m \cdot K$).

Nusselt number can be referred to as the ratio of convective to conductive heat transfer across a boundary where flows of convective and conductive heats are parallel and normal to the boundary surface.

Especially in natural free convection, nondimensional number called *Grashof* number takes the role to decide whether the flow is laminar or turbulent. The number represents the ratio of buoyancy force to the viscous force, and it is defined as follows [19].

$$Gr_L = \frac{g \cdot \beta(T_s - T_\infty) \cdot L_c^3}{\nu^2} \quad (3.8)$$

where g is the gravitational acceleration (m/s²),

β is the volume expansion coefficient (K⁻¹),

T_s is the surface temperature (°C),

T_∞ is the fluid temperature sufficiently far from the surface (°C),

L_c is the characteristic length of the geometry (m), and

ν is the kinematic viscosity of the fluid (m²/s).

Another important nondimensional parameter in natural convection is *Rayleigh* number which characterizes the relationship between buoyancy and viscosity as follows [19].

$$Ra_L = Gr_L \cdot Pr = \frac{g\beta(T_s - T_\infty)L_c^3}{\nu^2} Pr \quad (3.9)$$

where Pr is *Prandtl* number.

Prandtl number tells us the ratio of the molecular diffusivity of momentum and the molecular diffusivity of heat. The lower the Pr , the higher the diffusivity of heat ($Pr \ll 1$) and the higher the Pr , the lower the heat diffusivity ($Pr \gg 1$)[19].

The concept of boundary layer must be also introduced to describe heat transfer near the surface. This thin layer of fluid close to the wall is in contact with the moving fluid where the velocity of the fluid is assumed to be zero at the wall. It is called a no-slip condition. Under this premise, differential equations of mass, momentum, and energy conservation are solved [20]. Further detailed boundary conditions of the study are described in section 5.2.

If there is a cooling system, forced convection is involved with the nonlinear analysis and CFD analysis. Hereunder are some examples of typical convective heat transfer coefficients [20].

- Free convection in the air: 5-30 W/m²·K
- Forced convection in the air: 100-500 W/m²·K
- Forced convection in water: 100-15000 W/m²·K

3.3 Radiation

Radiation is the heat energy emitted from bodies in the form of electromagnetic waves or photons. It is deeply related to the changes in electronic configurations of the molecules or atoms [19]. Every object that has the absolute temperature above zero *Kelvin* radiates heat energy. This wave can travel even in the vacuum space where no medium exists. Since it travels in a speed of light, it is the fastest way to transfer heat.

All solids, liquids, and gases emit, transmit, or absorb radiation in different degrees. If any object is in contact with fluid, radiation and convection should be considered together, especially when ΔT is large enough. Unlike conduction and convection which are referred to as transport phenomena occur through volume, radiation is a surface phenomenon. Radiation occurs in the wide range of wavelengths and frequencies between 0,1 and 100 μm which covers ultraviolet, visible and infrared region [20].

Stefan-Boltzmann's law defines the total radiated energy of the black body (E_b). The black body is assumed to emit and absorb the maximum radiated amount under the given temperature and wave as follows [20].

$$E_b = \sigma \cdot T^4 \quad (3.10)$$

where $\sigma = 5,67 \times 10^{-8} \text{ W/m}^2 \cdot \text{K}^4$ and it is called a *Stefan-Boltzmann* constant.

A term called radiosity is used in the surface to surface radiation. Radiosity is defined as total energy leaving a surface per unit area and per unit time, thus includes both radiations emitted by the surface and the radiation reflected by the surface [19].

$$J_i = \epsilon_i E_{bi} + \rho_i G_i \quad (3.11)$$

where J_i is the radiosity on surface i (W/m²),

ϵ_i is the emissivity on surface i ,

E_{bi} is the blackbody emissive power of surface i (W/m²),

ρ_i is the reflectivity of surface i , and

G_i is the irradiance (W/m²).

For other bodies, radiation flux is defined as [20]

$$q = \sigma F(\epsilon T^4 - \alpha T_a^4) \quad (3.12)$$

where F is a radiation view factor,

ϵ = emissivity,

α = absorptivity,

T is the body temperature, and

T_a is the air temperature in K.

Since we are dealing with the 4th power term of temperature in the governing equation, there is a considerable amount of heat transfer even with a small temperature difference as well as a high-level nonlinear phenomenon which requires a heavy-duty computation. Similar to convection, radiation also happens in the boundary face of the body, however, it is a directional quantity based on the view factor as well as how the surface absorbs, reflects, and transmits the heatwave.

4. LAB EXPERIMENT

A lab experiment is carried out for the following purposes.

- To obtain the exact power losses due to copper losses and iron losses.
- To validate the simulation result of the surface temperature and to verify the transformer parameters.

To achieve these, three experiments in the subsequent sections are performed and discussed based on the model transformer with the following specifications.

- Rated output: 0,5 KVA
- Rated voltage: 110 V / 380 V
- Rated current: 2,62 A / 0,76 A

From the visual inspection of the wire connection, it is observed that LV (low voltage) side has a Delta connection and HV (high voltage) side has a Star connection. Winding resistance is measured by taking the resistance value between each line as follows.

- LV: 1,7 Ω
- HV: 16,3 Ω

4.1 No-load test (Open circuit test)

The aim of the open-circuit test is to experimentally measure the iron losses in the core part. This is done by applying a rated voltage on one side to generate flux while the other side of the circuit is opened. No current flows on the opened circuit side, thus no load is applied. So all power measured should be equal to the iron losses.

It is common to apply rated AC power on LV side and leave HV side opened since it is easier and safer using lower voltage instead of the higher one. Dual wattmeter method is a typical way to obtain the total power loss measurement from the 3 phase circuit. This method does not provide the power on each phase but offers a convenient way to measure the total power of the 3-phase circuit. The following is the circuit connection diagram for Star connection.

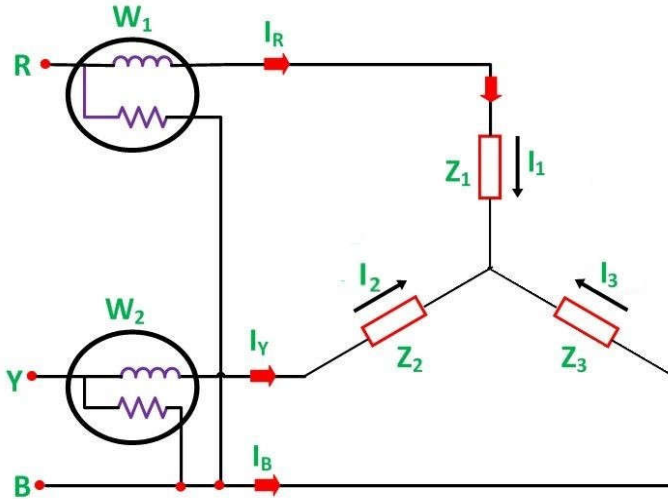


Figure 4.1 Two-wattmeter method for Star connection [21]

The sum of two powers measured from wattmeter 1 and 2 represents the total iron losses of the transformer.

$$W_o = W_1 + W_2 = V_1 \cdot A_1 + V_2 \cdot A_2 \quad (4.1)$$

where W_o is the total power (sum of W_1 and W_2)

V_1 is the line voltage between R and B

V_2 is the line voltage between Y and B

A_1 is the line current between R and B

A_2 is the line current between Y and B

Total power, the sum of the readings from W_1 and W_2 , represents the sum of copper losses and iron losses which can be written as

$$P_{Fe} = W_o - P_{Cu} = W_o - (I_o^2 \cdot R_{eq}) \quad (4.2)$$

where I_o is the no-load current

R_{eq} is the equivalent resistance.

When the applied current is minimal, the second term, $I_o^2 \cdot R_{eq}$ is usually negligible yielding

$$W_o = W_1 + W_2 \approx P_{Fe} \quad (4.3)$$

On the 3 phase power supplier connected to the LV side, the voltage is raised from 0 V to 110 V while the HV side remained open. Upon LV side reaching similar to the rated voltage, the measured losses from the 2 wattmeters are taken as follows;

Table 4.1 No-load test measurement

LV	Wattmeter 1		Wattmeter 2		Sum
	W1	-14,5 W	W2	1,5 W	13 W
V1	110,7 V	V2	109,6 V		
I1	0,184 A	I2	0,231 A		

When performing the actual experiment, slight unbalance of voltage (about 1 V) and low resistance in the neutral cable was detected which lead to a remarkable current unbalance between 2 wattmeters. The P_{Fe} value of 13 W is applied as iron losses.

It is known in general that no-load current is approximately 3% to 5% of the full load current and it is constant regardless of the load [13].

4.2 Short circuit test (Impedance test)

The main principle of the short-circuit test is to apply rated current on one side while short-circuiting the other to measure the copper losses caused by joule heating. Short circuit test can be performed on either side. The test is performed on both side but only the HV side measurement is presented here. More data on both sides are given in the appendix. Circuit diagram of 2 wattmeter method on Delta connection for HV side is presented as follows.

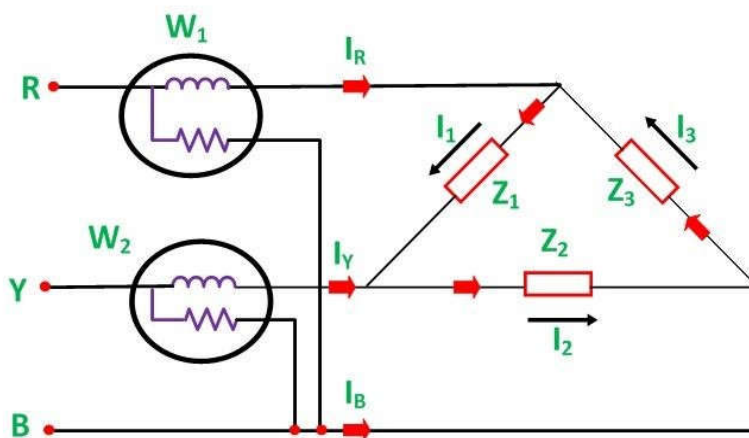


Figure 4.2 Two-wattmeter method circuit for Delta connection [21]

The voltage is applied to the high voltage side and the power, ampere, and voltage are measured. The voltage is set to be zero and gradually increased until the current reaches to its rated current, that is $I_1 = 0,76 \text{ A}$.

Since the applied voltage will remain minimal when the full loaded current is reached, the power measured at this point can be referred to as resistive losses in copper windings.

Table 4.2 Measurement readings from 2 wattmeters for short-circuit test

HV	Wattmeter 1		Wattmeter 2		Sum
	W1	17 W	W2	15 W	32 W
V1	24,5 V	V2	24,1 V		
I1	0,76 A	I2	0,76 A		

The copper losses of total 32 W is obtained and this will be used as the value of P_{Cu} .

4.3 Load test and temperature measurement

The surface temperature of the fully-loaded transformer is measured with the loader connected. The load test is carried as a step-up device (Star-Delta) since the loader responded well with a step-up connection. It is also mentioned in the earlier chapter that Star-Delta connection is usually intended for a step-up transformer.

3 phase power is supplied to the LV side and the loader is connected to the HV side with 2 wattmeters connected on each side to ensure the rated input and output are applied on both sides. The loader is located far away from the transformer so that the heat dissipated from the loader will not affect the measurement of the surface temperature.

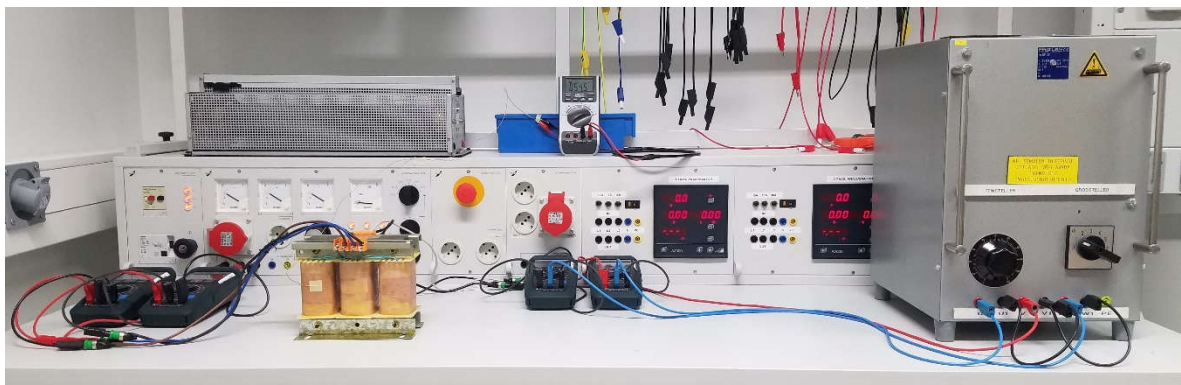


Figure 4.3 The entire view of the load test

The measurement is carried out for a total 260 minutes with the temperature measurement interval of every 20 minutes. The laboratory room temperature is measured to be 22.3 °C.

A resistive load is applied so that the model transformer is fully loaded as shown in Table 4.3. A voltage drop about 21 to 25 V is detected due to the inefficiency of the device. The transformer efficiency is calculated to be 91,3%.

Table 4.3 Readings of 2 wattmeters for the load test

	Readings from 2 Wattmeters				
	V1	V2	A1	A2	Input/Output
LV	112,2 V	110,3 V	2,69 A	2,68 A	0,515 kW
HV	359,0 V	354,6 V	0,77 A	0,75 A	0,47 kW

A thermocouple with the following specification is attached to the centre of the left winding surface to verify and compensate the error read from the thermal image camera (FLIR E50). The temperature values are indicated through a multimeter.

- Thermocouple type: K
- Temperature range: -200 °C ~ 1250 °C
- Chromel (yellow): positive, Alumel (red): negative

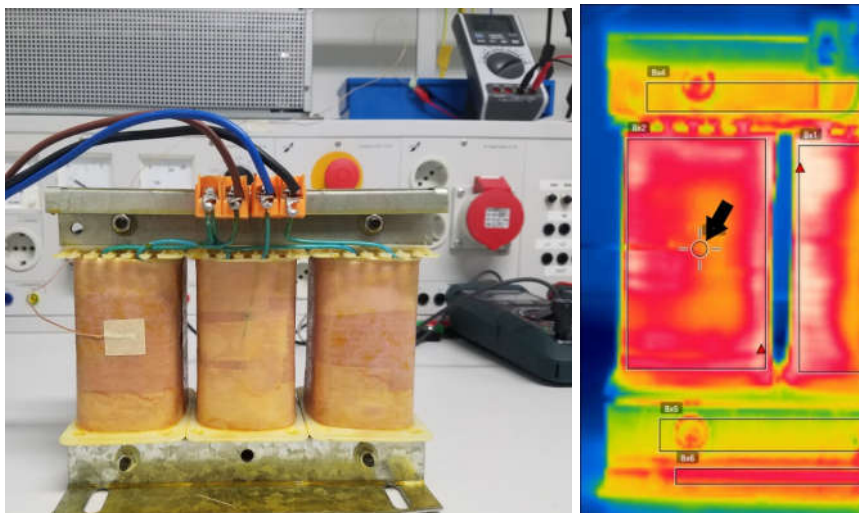


Figure 4.4 The location of the thermocouple on the transformer and the thermal image

A spot temperature read from the same position of the thermal image is compared. For total 14 times of measurements and comparing the temperature difference between the thermocouple and the thermal image spot as shown in Figure 4.4, the

average temperature deviation is 0,3 °C which is agreeable that the self-calibrating thermal camera does not require further compensation for the experiment.

4.3.1 Uncertainty

Temperature measurement of IR thermal image camera is based on the measured radiation and the internal camera calibration. Both thermal image and the thermocouple readings provide 0,1 °C of accuracy. Accuracy information of a thermal image camera FLIR E50 is found in the user's manual [22] as follows.

- Object temperature range: 0 °C to +650 °C (or -20 °C to +120 °C)
- Accuracy: ±2 °C or ±2 % of reading for ambient temperature 10 °C to 35 °C.

According to the manufacturer[23], the followings are the parameters affecting the accuracy of the IR camera.

- Emissivity,
- Reflected ambient temperature
- Transmittance
- Atmosphere temperature
- Camera response
- Calibrator (blackbody) temperature accuracy

Taking all partial error factors, root-sum of squares (RSS) method is used to calculate the total errors of the IR camera using

$$Total\ error = \sqrt{(\Delta T_1^2 + \Delta T_2^2 + \Delta T_3^2 + \dots \Delta T_n^2)} \quad (4.4)$$

where ΔT_n is the temperature error measured on each parameter.

Therefore, the maximum uncertainty of the IR camera is expected to be within ±2 °C. However, as mentioned previously, the average temperature difference between the thermocouple and the thermal image spot is 0,3 °C.

4.3.2 Experiment results

4 points of interest with high temperatures observed are extracted from the thermal image by post-processing all images using FLIR tool software. They are depicted on the following table. Further detailed data table on other parts are attached in the appendix.

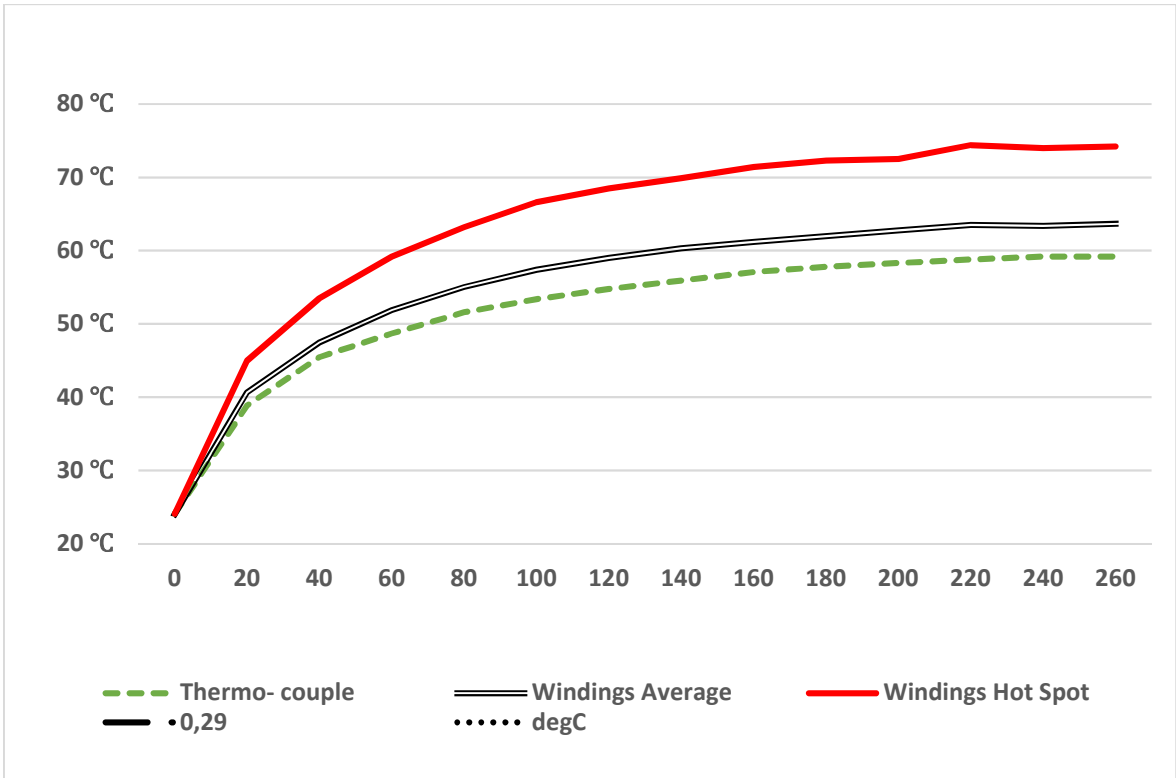


Figure 4.5 Measured surface temperature in different areas of the transformer

As shown in Figure 4.5, the temperature rapidly rises during the first 40 minutes and the gradient becomes moderate after. Hot spots on the winding part reach up to 74.2 °C at the end which is the maximum temperature detected from the entire transformer surface. Frame top part shows the lowest temperature as it is more exposed to the ambient air.

After more than 4 hours of experiment, over 40 thermal images were taken and post-processed to retrieve temperature data. Among them, only the final ones which show the final thermal equilibrium state are presented hereunder as they are of the most concern.

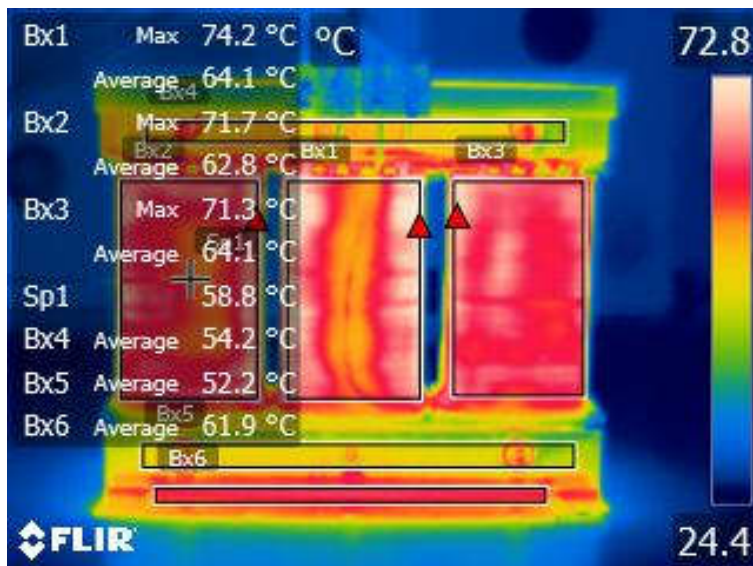


Figure 4.6 Front view of thermal images taken at 260 min.

A thermal image taken at 260 min. is shown in Figure 4.6. Hot spots (marked in the red triangle on white colour) are mostly found on the edge of the windings where more tension is applied on the cellulose cover of the windings. Close thermal contact between the copper winding inside and the cellulose cover might lead to more vigorous heat transfer through the boundary layer. The white colour areas are also concentrated on both sides of the middle winding (Bx1). It reflects that the radiation from the other windings and hot air congested between the winding might cause this phenomenon. Another reason for hotspot can be explained due to the irregularity in the windings. Although copper wires might be wound evenly with constant tension during the manufacturing process, extra wires that cross over the primary and secondary windings to the terminals make irregular surface beneath the cellulose cover. This can be observed even from the thermal images (the middle winding). More air pocket renders more room for airflow that make uneven distribution of temperature as well as bring down the surface temperature.

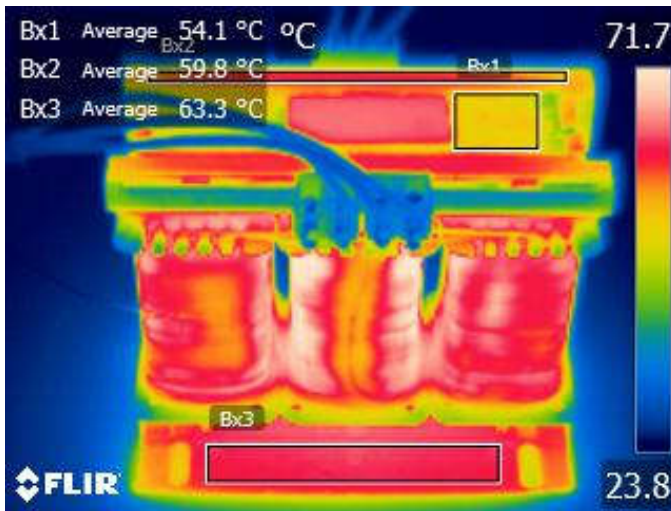


Figure 4.7 Top view of the thermal image taken at 260 min.

As shown in Figure 4.7, a relatively high temperature is discovered at the foot frame part (Bx3) that is over 63 °C. Normally, more heat would be applied to the upper part due to a buoyancy characteristic of convection. However, heat is rather trapped between the floor and the epoxy laminated surface of the foot frame. Unlike the top frame which is bare sheet metal, a laminated surface has different surface emissivity and convective heat transfer rate resulting in higher surface temperature. It should also be considered that there is a long square hole on the top part the frame to cool out the heat. All these have contributed to bringing down the surface temperature of the top frame more than the foot frame.

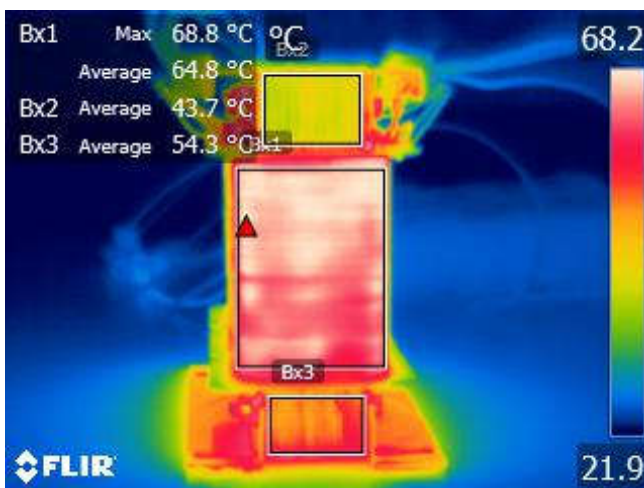


Figure 4.8 Side(right) view of the thermal image taken at 260 min.

A thermal image taken from the side is shown in Figure 4.8. Similar to the frame part, side of the core bottom (Bx3) shows the higher temperature of 54,3 °C than the side of the core top (Bx2) that has 43,7 °C showing a distinctive temperature difference of

10,6 °C. Assuming that the conduction process is regular inside the core, there could be few assumptions as follows.

- Heat is trapped between the floor and the frame: Heat transfer rate of the floor is not high enough to dissipate heat.
- Foot frames are not cooling enough compared with the upper frames: It is also discovered that much portions of the foot frame surfaces are coated with some epoxy material which is alleged to block the heat dissipation to the air.
- Top frames have long square holes on both sides meant to cool out the hot air which would bring down the temperature.

All these factors have overwhelmed the buoyancy effect of convection making upper part cooler than the lower one.

5. Heat Transfer Model

Comsol Multiphysics® is a FEM software which can combine modelling and simulation for many different scientific problems by solving partial differential equations in coupled systems. The main reason to use this software is associated with the license granted to the institution and the further coupling possibility with the electromagnetism and joule heating model.

The Iron losses and the copper losses are measured experimentally, and the measured heats in Watt will be assigned to the copper winding domain and the steel core domain respectively. These will act as heat sources and the FEM tool will simulate the heat transfer analysis according to the geometry and the materials. All three modes of heat transfer, conduction, convection, and radiation are modelled including the ambient air domain. The transformer being exactly symmetric in the width, it is efficient and time-saving to cut the model into a half to make the model axisymmetric.

5.1 Geometry and material property

Detailed geometry of the full 3D model is created as shown in Figure 5.1. Some simplification is made by eliminating the minor surface to prevent complicated mesh being crashed.

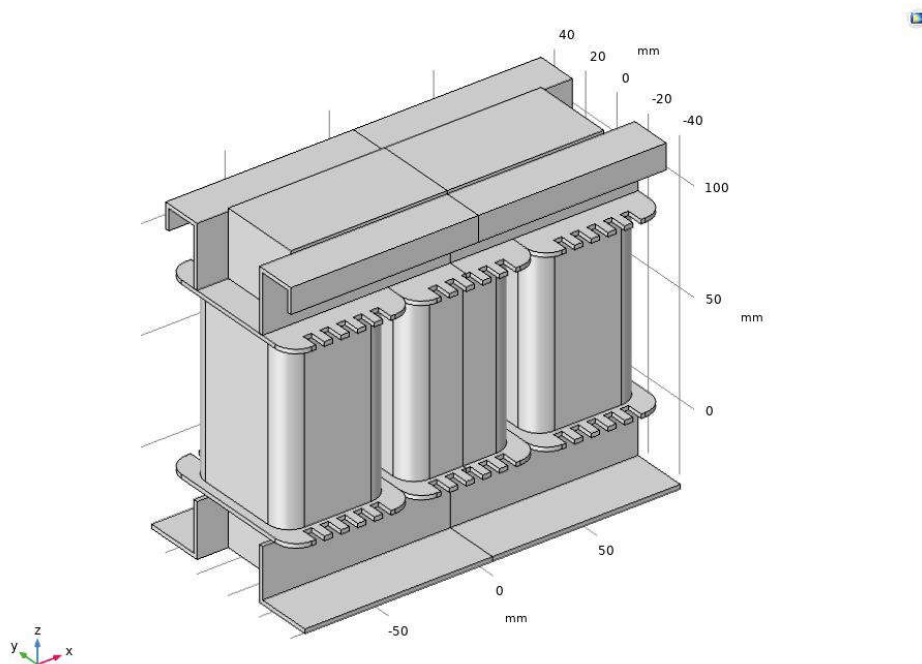


Figure 5.1 Full3D view of the transformer model

Main properties of the major materials assigned are shown in Table 5.1 and Table 5.2 respectively.

Table 5.1 Material properties of the main parts

Parts & Materials		Windings	Ecore	Steel Frame	Bobbin
Properties & symbols		Copper	Laminated Steel (3%)	Sheet metal	Zenite
Density	ρ	8940 kg/m ³	7650 kg/m ³	7870 kg/ m ³	1620 kg/ m ³
Heat capacity	C_p	385 J/(kg·K)	600 J/(kg·K)	440 J/(kg·K)	125 J/(kg·K)
Thermal Conductivity	k/k_n	400 W/(m·K)	28 / 3,37 W/(m·K)	76,2 W/(m·K)	0,32 W/(m·K)
Electric Conductivity	σ	6,00E+10 S/m	1,72E+06 S/m	1,12E+07 S/m	-
Relative permeability	μ	1	1500	4000	-

Table 5.2 Properties of air at given temperature

Air properties & symbols	Unit	Values
Temperature	T	290 300
Density	P	1,218 1,177
Specific heat	C_p	1,006 1,006
Thermal conductivity	k	0,025 0,026

5.2 Boundary conditions

Since we are dealing with all 3 modes of heat transfer in both solids and fluid, the boundary conditions and governing equations should be properly defined satisfying the energy balance equation. It can be stated that the total heat transfer to the surface in all modes should be equal to the total heat transfer from the surface in all modes [19].

Conduction dominates the heat transfer inside the opaque solids whereas both convection and radiation take places on the surface where the solid and the air meets. Therefore, it can be described by inward and outward regions of the boundary.

As for inward, the boundary between the winding and the E-core is set as a thermal contact specified as an equivalent thin resistive layer with a thickness of 2 mm which is the thickness of the bobbin. The copper windings and the E-core are uniform

volumetric heat sources(Q_0) that exert constant heat energy through the surface. It is the heat loss values gained from the experiment and divided by half since the model is axisymmetric. Corresponding governing equations according to the boundaries are listed in Table 5.3.

Table 5.3 Boundary conditions and governing equations

Boundary	Governing equations	Remarks and references
Heat Sources	$Q_0 = \frac{P_0}{V}$	For Winding & E-core volume $P_0 = P_{cu}/2$: the total heat energy (W)
Solids and fluid	$\dot{\mathbf{q}} = -k\nabla T$ $\rho C_p \mathbf{u} \cdot \nabla T + \nabla \dot{\mathbf{q}} = Q$	For windings, core, frames, bobbins Equation (3.5) and (3.6)
Surface to ambient radiation	$-\mathbf{n} \cdot \dot{\mathbf{q}} = \epsilon \sigma (T_{amb}^4 - T^4)$	For all surfaces in contact with the air Equation (3.12)
Surface to Surface Radiation	$J_i = \epsilon_i E_{bi} + \rho_i G_i$ $E_{bi} = \sigma T_i^4$	For surfaces viewing each other Equation (3.10) and (3.11)
Heat flux in the air and the floor	$-\mathbf{n} \cdot \dot{\mathbf{q}} = q_0$ $q_0 = h(T_{amb} - T)$	For the air domain to the outer air Equation (3.6) h value is calculated and decided by the geometry of the air domain and the floor (Cylinder and horizontal plate respectively)
Turbulent flow	$\rho \frac{\partial \mathbf{u}}{\partial t} + \rho(\mathbf{u} \cdot \nabla)\mathbf{u}$ $\rho \frac{\partial k}{\partial t} + \rho(\mathbf{u} \cdot \nabla)k$ $\rho \frac{\partial \epsilon}{\partial t} + \rho(\mathbf{u} \cdot \nabla)\epsilon$	Time averaged continuity, momentum, and thermal energy equations for incompressible flow: RANS, k - ϵ model is applied [20]

All material property values are taken from Table 5.1 and Table 5.2. Additional boundary conditions are stated hereunder.

- Ambient air temperature is 23 °C
- The initial surface temperature of the device is 24 °C
- Air pressure is 1 atm.

- Anisotropic conduction in the solid is applied in the E-core so that different conductive heat transfer coefficients are applied.
- The control volume of the air domain is considered a steady state so that the total energy change in the volume is set to be zero ($\Delta E_{cv}=0$).

Surface emissivities of each boundary are set as follows.

- Bobbin (Zenite 7130): 0,7
- Winding cover (Cellulose): 0,75
- E-core (Silicon Steel): 0,8
- Frame (top): 0,25 / (foot): 0,3
- Floor (3 Poly laminate): 0,8

5.3 Heat sources and air domain

Two heat sources are modelled in the copper windings and the E-core. One is the resistive losses in the copper windings and the other is the core losses in the E-core. Using equations (2.9) and (2.10), calculation of copper losses is modelled, however, the data for the exact number of turns in the winding is not available from the manufacturer. Therefore, the power losses values obtained from the experiment are assigned as follows.

- Copper losses: $P_{Cu} = 32 \text{ W}$
- Iron losses: $P_{Fe} = 13 \text{ W}$

The above volumetric heat energy assigned in the domain is distributed evenly and exert heat until the surface temperature reaches the equilibrium with heat dissipation to the ambient air. This enables the model to be a simpler and less expensive simulation, however, disables analyzing thermal dynamics of the copper winding inside or surface such as depicting hot spot over the winding surface. The copper winding and the E-core is designed as solid to make the geometry and simulation simple and light-weight.

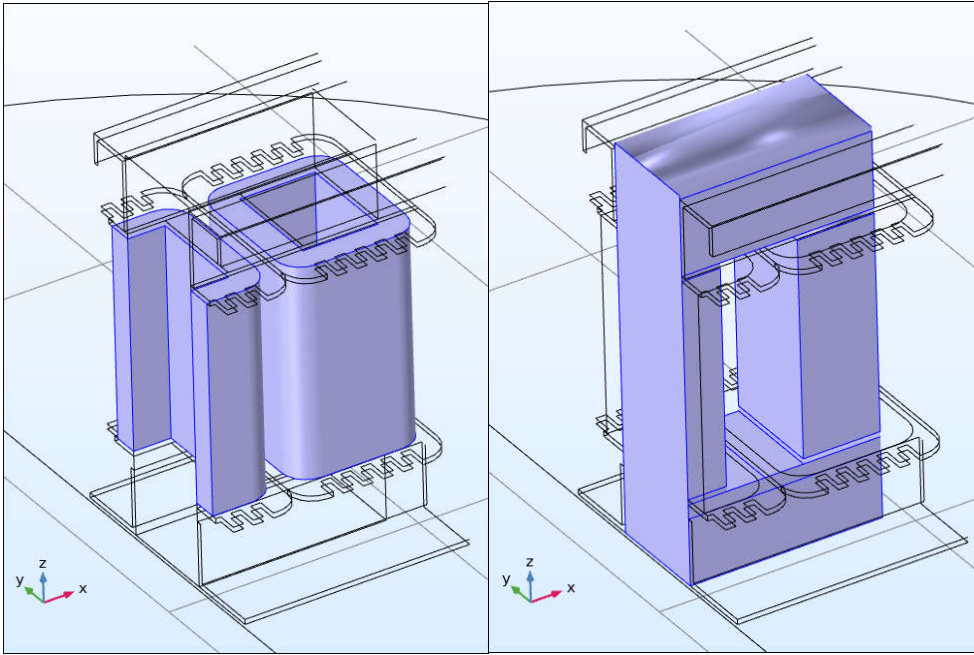


Figure 5.2 Two heat sources modelled - copper windings and E-core

This approach is more realistic and makes the model solvable not only because of the simple and less expensive simulation but also the fact that the thin sheet metals and multi-turn coils with fine thickness would require tedious work on meshing.

Bobbin with a thickness of 2 mm should also be considered as it affects the heat transfer simulation. However, because adding thin layered material with complicated geometry leads to a heavy model and requires finer mesh, some simplification is made by replacing thin layered geometry with boundaries. Comsol features assigning material properties to the boundary surface. 4 inner faces between the copper winding domain and the E-core domain are assigned as inner bobbin boundary which will obey the properties of the bobbin material.

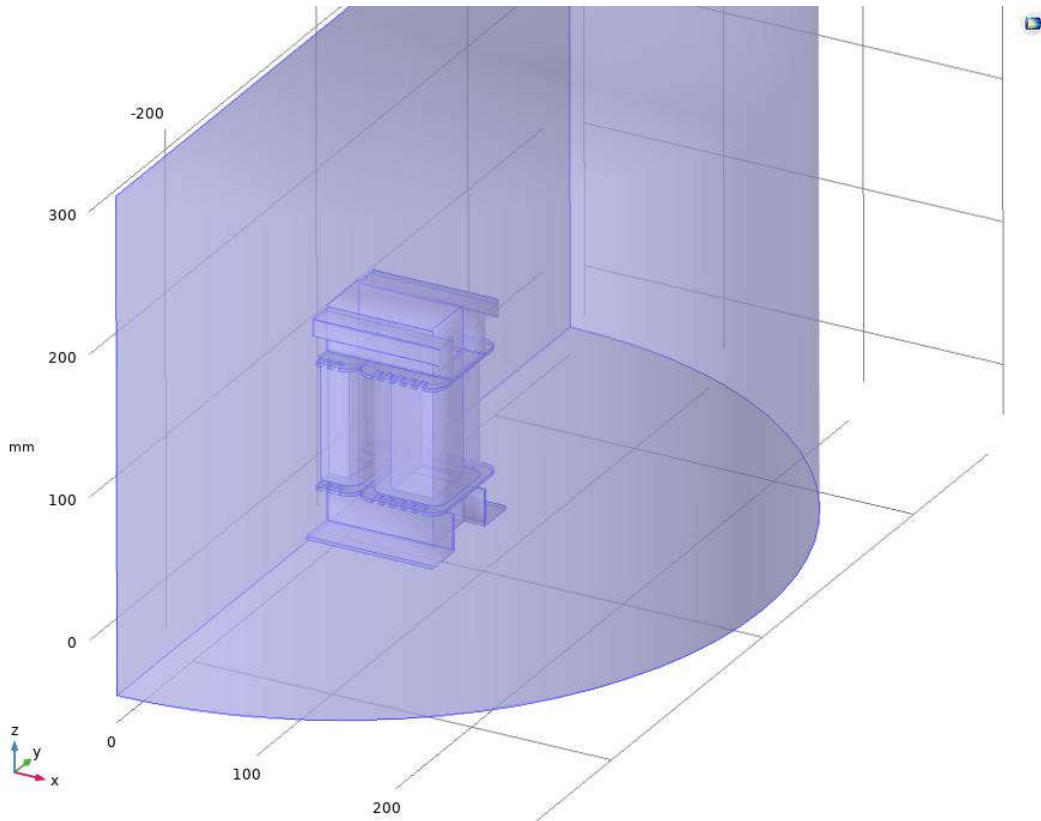


Figure 5.3 Entire view of the model of the transformer in the air domain

As shown in Figure 5.3, the ambient air domain is created to accurately model and calculate the heat transfer throughout the ambient air. Finding the correct value of heat transfer coefficient (h) between boundaries is not easy in the real world physics because all geometry and material properties are interrelated to each other and they also differ along with the temperature change. Hence, in order to properly calculate the heat transfer rate between boundaries, the solid material surface should be placed in the surrounding ambient air.

The followings are the assumption of the surrounding air domain.

- Surface to surface radiation and surface to ambient radiation are considered.
- The outer boundary of the ambient air is set as an open boundary so that there is a free mass flow in the air.
- There is no viscous stress along the open boundary.

5.4 Anisotropic heat transfer in the E-Core.

The transformer core consists of multi-layers of laminated soft steel is designed to minimize eddy current losses and hysteresis losses. It provides a low reluctance path

to the flow of the magnetic flux as well. Each soft metal sheet is laminated to prevent any current flow between sheet metals, the direction normal to the plate.

Similarly, conductive heat transfer in the transformer core with the multi-layers of laminated steel shows similar behaviour as electrical conductivity. Unlike solid steel where heat propagation shows an isotropic pattern, a heat transfer rate of laminated steel along the plate is much higher than the direction normal to the plate that is across the sheet metals. Therefore, to achieve more realistic result avoiding heavy computational load, anisotropic heat conductivity is applied in the form of a matrix for the steel core domain as follows.[24]

$$K = \begin{bmatrix} k_{xx} & 0 & 0 \\ 0 & k_{yy} & 0 \\ 0 & 0 & k_{zz} \end{bmatrix} \left(\frac{W}{m \cdot K} \right) \quad (5.1)$$

In this study, plane surfaces of the sheet metals are positioned on the x-z plane and piled up along the y-axis. The transverse conductivity through laminated layers is much smaller than the one along the plane, thus $k = k_{xx} = k_{zz}$ and $k_n = k_{yy}$. The detailed values are presented in Table 5.4.

Table 5.4 Heat transfer characteristics of laminated steel(3%) [25]

Properties of laminated electrical steel (3% Si)			
Thermal Conductivity, k	28 W/m·K	Density, ρ	7650 kg/m ³
Transverse Thermal conductivity, k_n	3,37 W/m·K	Specific heat, C_p	600 J/kg·K

In general, the difference in conductivity values is not depended on the thickness of the sheet metal but rather on the thickness of the lamination [26].

5.5 Meshing

As the geometry of the model gets complicated, detailed meshing process is a must because most meshing algorithm in CFD tools is sensitive to the model geometry topology. Unnecessary boundaries and edges should be removed using virtual operations to prevent any possible crash over the boundary layers.

To start from two main heat sources which are the copper windings and E-core, inner bobbin boundary which lie between these 2 heat sources is configured first marked with blue colour in Figure 5.4.

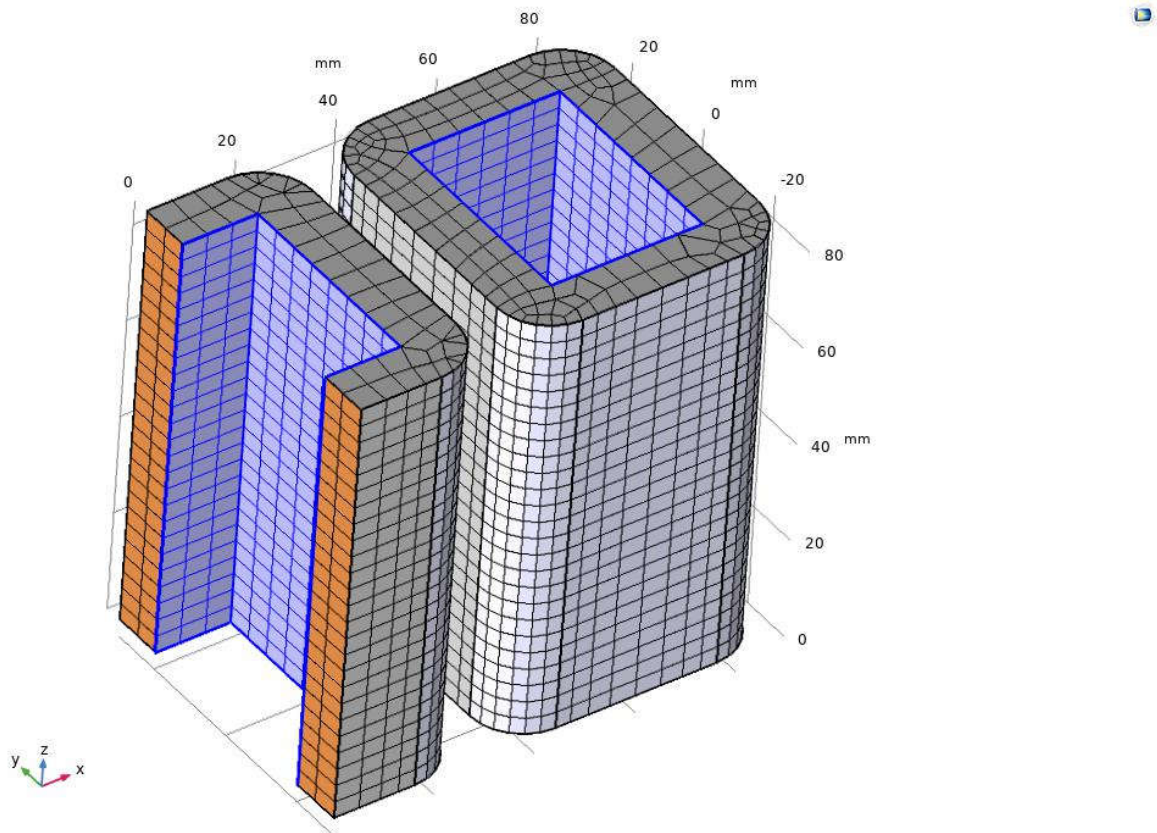


Figure 5.4 Quad mesh generated in the winding and E-core domains

The free quad mesh is applied on this boundary between copper windings and the inner bobbin wall. Then the mesh is swept to the copper winding domain to generate hexahedron shaped mesh. Quad mesh complies well with the general shape of the copper windings and the E-core leg that penetrates through the windings.

Another free quad mesh is applied on the surface of the E-core as shown in Figure 5.5. Then it is swept inwardly through the entire domain. The quad mesh is expected to perform an effective calculation over the shape of the E-core domain where anisotropic heat transfer rate is applied. The size of the quad mesh gets smaller and the shape gets irregular at the filleted areas around the corner, the sharp edges and vertices.

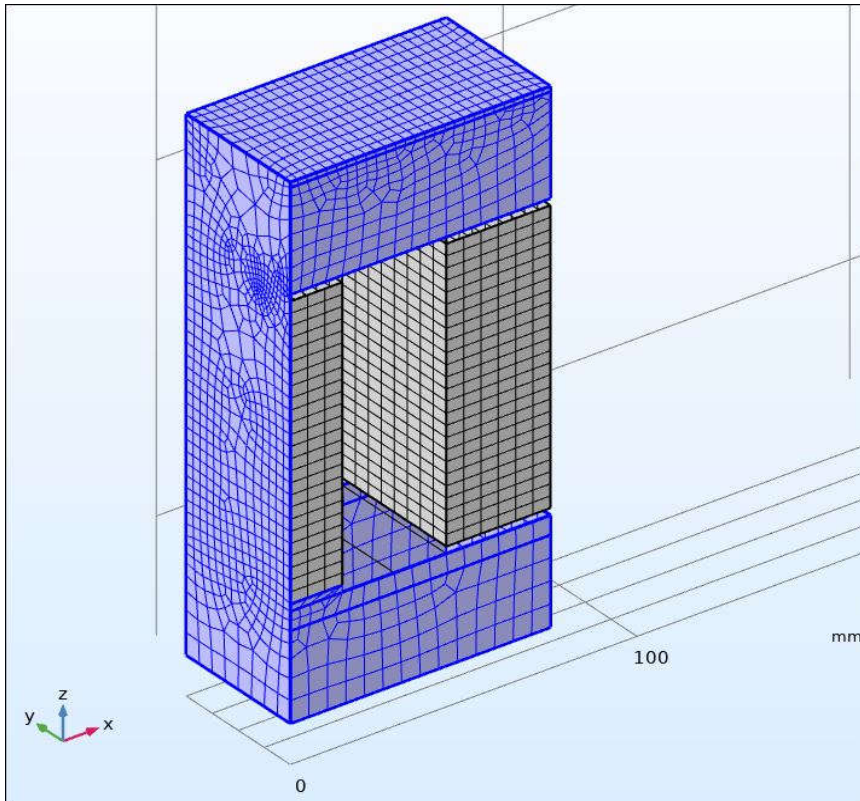


Figure 5.5 Quad mesh generation on the E-core

The free tetrahedral mesh is applied for the rest of the parts such as bobbin and frame parts. The mesh sizes are predefined according to the importance. For example, the coarser mesh is applied to the domain where heat transfer impact is less significant than copper windings and the core. These domains, such as bobbin and steel frame, have geometry with thin layers with a thickness of 1 or 2 mm. Regardless of the mesh size assigned for a specific domain or boundary, a finer mesh is automatically applied to the sharp corners and edges to cope with the acute geometry. Figure 5.6 shows the combination of free quad mesh and free tetrahedral mesh over the entire transformer model.

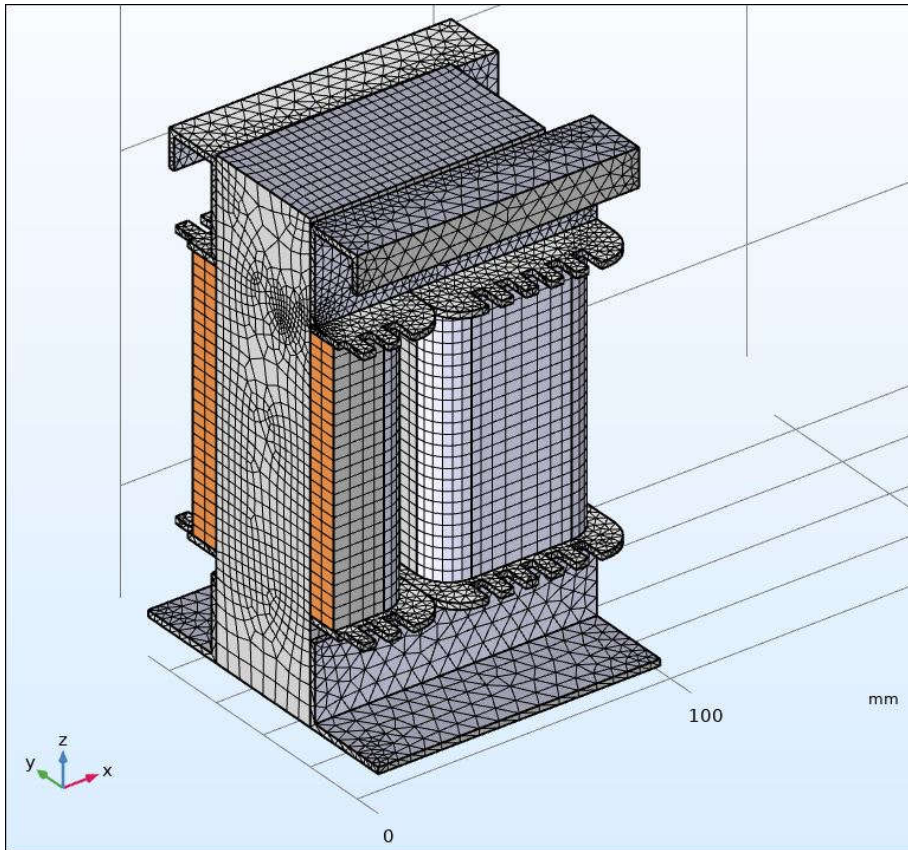


Figure 5.6 Free quad and free tetrahedral mesh of the entire transformer model

In the case of the air domain, additional setup is required especially in the area where a narrow gap between windings is and where air contacts with sharp edges of the transformer surface. This area requires finer mesh than the farther region. So the element size is customized from a minimum 2 mm to maximum 30 mm. As can be observed from Figure 5.7, mesh size is smaller adjacent to the device but gets bigger as it goes farther. Utilizing this kind of meshing technique offers a remarkable reduction in simulation load and time. Some minor error might appear while generating mesh but it could be resolved by adjusting the element size and performing the extra virtual operation. The entire views of the mesh modelled including the ambient air domain are shown in Figure 5.8.

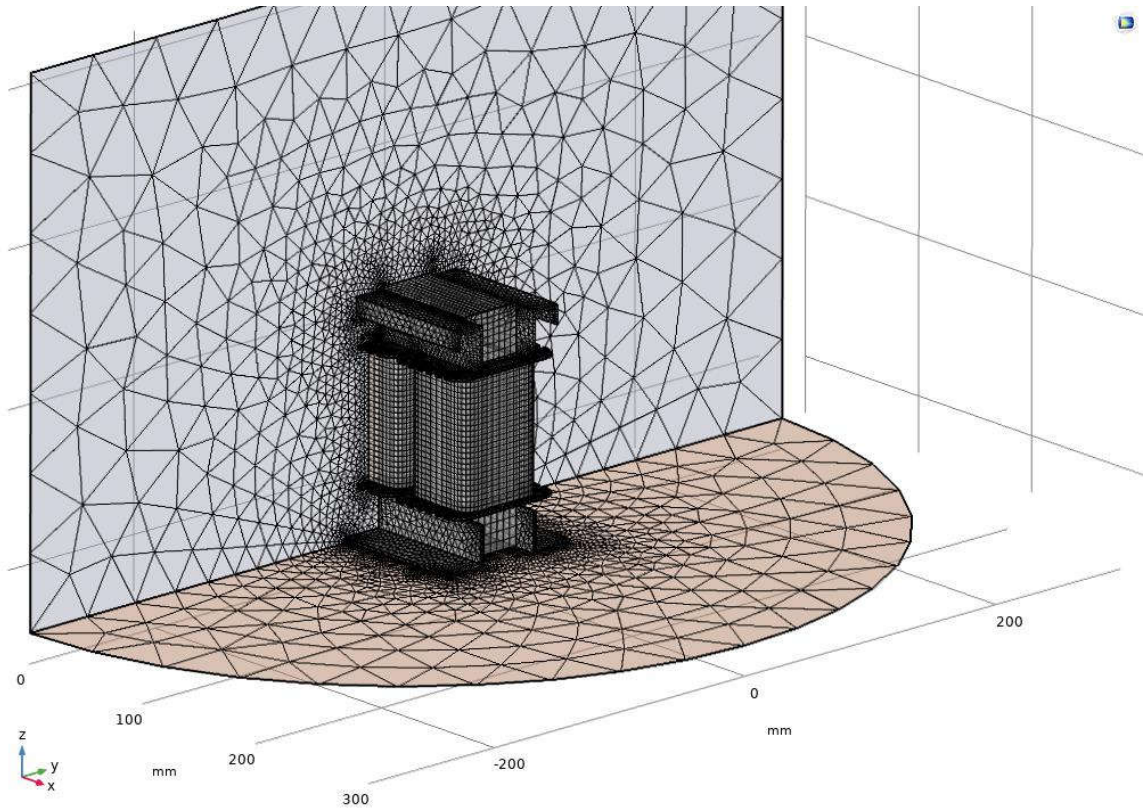


Figure 5.7 Cut-view of the air domain

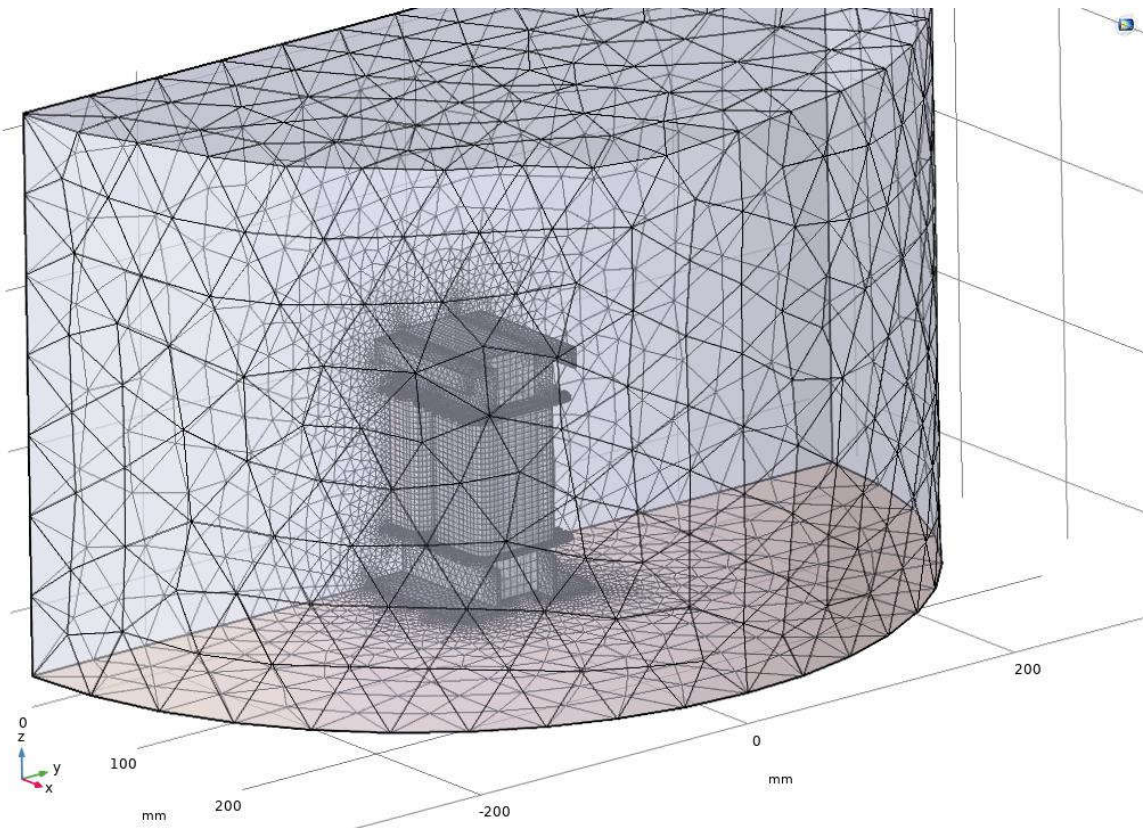


Figure 5.8 Entire view of the air domain

Finally, the mesh quality is speculated through the mesh generation statistics as shown in Figure 5.9.



Figure 5.9 Statistics on mesh generation and histogram

There are total 267596 mesh elements generated in the model and the tetrahedral element is the majority for they suit well in the edges, corners, and narrow regions. Although the minimum element quality shows a value of 0,0002, the average value over 0,6 shows moderately enough quality of the mesh. It can be assumed that most of the low-quality meshes are formed in bobbins and frames because meshes for the windings

and E-core are extruded from the 2D surface instead of meshing directly in the 3D domain. This improves the mesh quality by generating regular mesh shape and size.

The quality measure histogram shown at the bottom of Figure 5.9 is based on the skewness which is a suitable measure for most types of element. Mesh element quality, a dimensionless quantity ranging between 0 and 1, represents the regularity of the mesh elements. 0 means the element is not generated and 1 means a perfectly regular element [27]. It is observed from the histogram that the quality distribution is concentrated on the right-hand side of the histogram where values are weighted to 1.

Mesh independent test is also performed by executing the simulation with the finer mesh and the coarser mesh. Although not globally, mesh element sizes are adjusted with several different combinations on important boundaries and domains and they return similar results.

6. Simulation result

Simulation is performed using Comsol Multiphysics®(ver.5.4). The simulation is set to be time-dependent as same as the experiment time scale from 0 to 260 min. with 20 min. interval. This study mode is more time-consuming and resource-intensive compared with the stationary mode, however, it is expected to provide more realistic results as well as the flow velocity field and pressure gradient according to time. The detailed thermal and electromagnetic parameters other than material properties are listed hereunder and the detailed geometric parameters are attached in the appendix.

Name	Expression	Value	Description
d	0.4 [mm]	4E-4 m	Coil diameter
I1	0.76 [A]	0.76 A	Current-Prim. winding
I2	2.26 [A]	2.26 A	Current-2nd winding
k	28 [W/m/K]	28 W/(m·K)	Therm. Conductivity of Elect. Steel
k_n	3.37 [W/m/K]	3.37 W/(m·K)	Transversal therm. conductivity
L_av	$2 \cdot (\text{windW} + \text{windD} + \text{windT})$	0.244 m	Average coil length of a turn
m_cu	$\rho_{\text{Cu}} \cdot N_p \cdot L_{\text{av}} \cdot S_c$	0.11264 kg	Copper winding mass
Np	410	410	No. of turns - primary
Ns	N_p / Tr	68.522	No. of turns - secondary
P_cu	$\phi^2 \cdot I_1^2 \cdot R_{\text{AC1}} + I_2^2 \cdot R_{\text{AC2}}$	31.993 W	Copper losses
P_fe	13 [W]	13 W	Iron losses
phi	3	3	Number of phase
R_AC1	$N_p \cdot (L_{\text{av}} - \text{windT}) / (\sigma \cdot S_c)$	12.729 Ω	AC resistance - primary
R_AC2	$N_s \cdot (L_{\text{av}} - 3 \cdot \text{windT}) / (\sigma \cdot S_c)$	1.9455 Ω	AC resistance - secondary
rho_Cu	8960 [kg/m ³]	8960 kg/m ³	Copper density
rho_Fe	7.65 [g/cm ³]	7650 kg/m ³	Steel density
Sc	$(d/2)^2 \cdot \pi$	1.2566E-7 m ²	Coil cross-sectional area
sigma	5.998e7 [S/m]	5.998E7 S/m	specific conductivity of copper
Tamb	23 [degC]	296.15 K	Ambient air temperature
Tr	$\sqrt{3} \cdot 380 / 110$	5.9834	Turn Ratio

Figure 6.1 Electromagnetic and thermal parameters set in Comsol

The simulation components include heat transfer in solids and fluids, the surface to ambient radiation, surface to surface to radiation, turbulent flow with gravity, and finally all heat transfer interfaces are to be coupled with the turbulent flow interface in the non-isothermal flow node. After a simulation time reaching over 3 hours and 6 minutes, the following results are achieved.

6.1 Temperature analysis

The axisymmetric surface temperature of the transformer is obtained as shown in Figure 6.2. The highest temperature is found in the overall surface of copper windings that is 67,3 °C and the lowest of 46 °C at the edge of the bobbin.

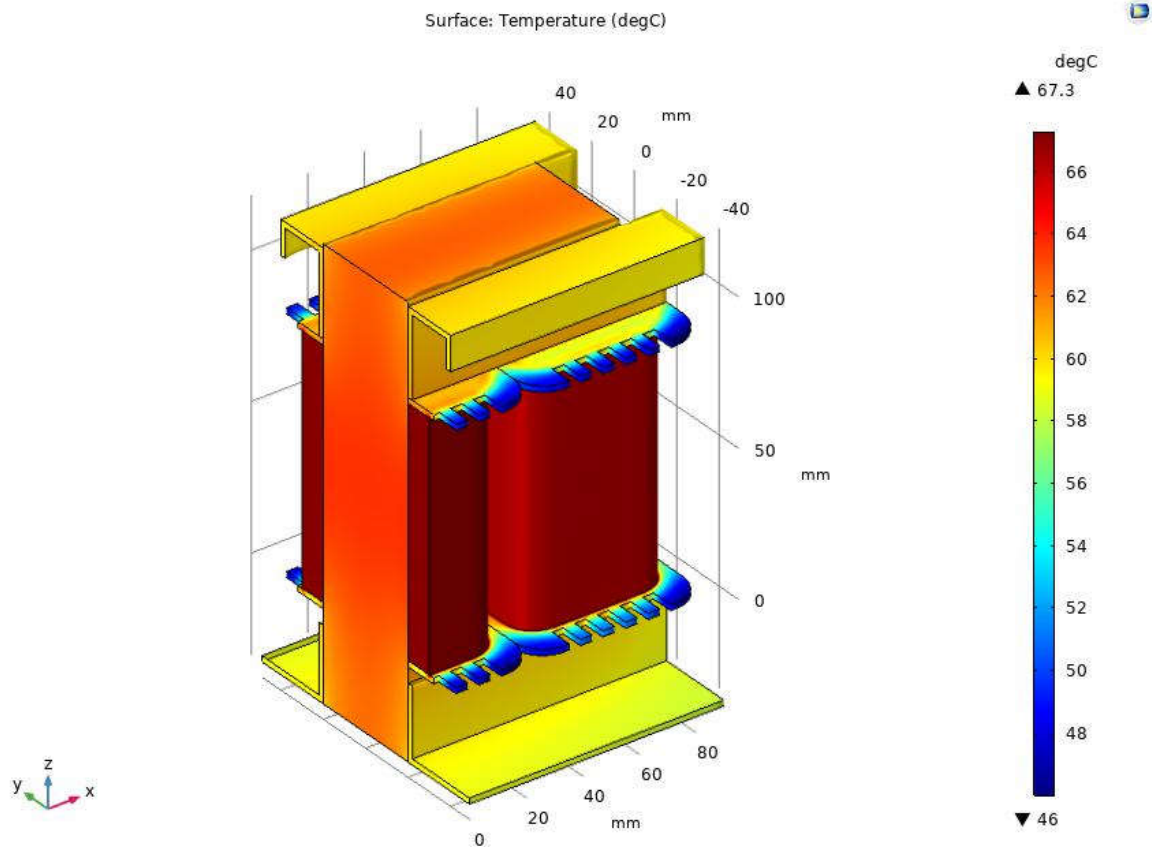


Figure 6.2 Surface temperature of the transformer shown in the axisymmetric view

The copper winding parts show almost uniform surface temperature since a lump sum amount of heat energy is directly assigned to the volume. From there, heat is transferred inward to the E-core, outward to the air, upward and downward to bobbins. More detailed values of maximum and minimum surface temperatures are listed in Table 6.1.

Table 6.1 Maximum and minimum surface temperature and locations

Surface Boundary	Winding	E-Core	Frame	Bobbin
Max. Temperature	67,3 °C	62,9 °C	61,7 °C	67,3 °C
x-coordinate (mm)	90,0	75,0	9,0	90,0

y-coordinate (mm)	49,0	20,0	4,9	40,0
z-coordinate (mm)	118,5	118,5	11,7	87,0
Min. Temperature	66,6 °C	59,2 °C	58,2 °C	46,0 °C
x-coordinate (mm)	0,0	0,0	0,0	0,0
y-coordinate (mm)	-30,0	-20,0	-4,9	-40,0
z-coordinate (mm)	0,0	-33,5	-33,5	-0,2

As can be seen from the table, the temperature difference between minimum and maximum is only 0,7 °C in the copper winding but 3,7 °C in E-core, 3,5 °C in Frame, and 21,3 °C in bobbin respectively. Bobbin which is in direct contact with the biggest heat sources but has the lowest thermal conductivity shows the extreme difference in temperature according to the position.

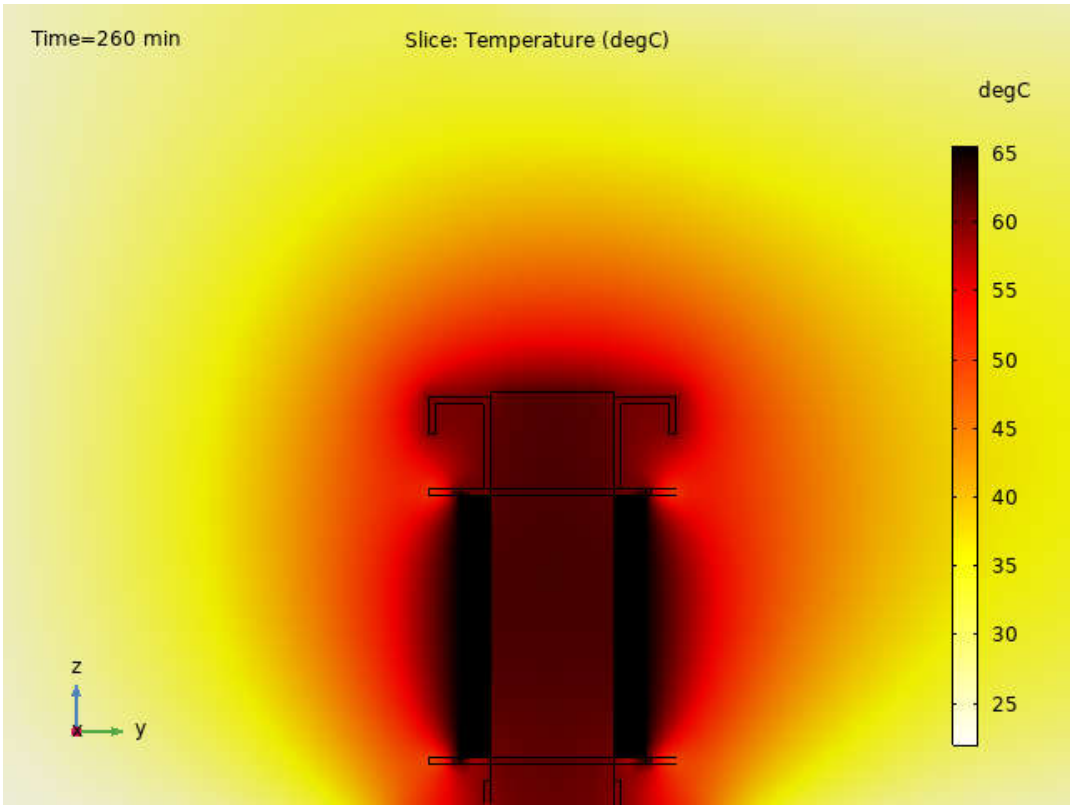


Figure 6.3 Heat propagation view on the y-z plane

Heat propagation shown on the y-z plane is shown in Figure 6.3. Heat propagation is observed on this plane from 3 main volumes that are upper core, winding, and the lower E-core to the ambient air. It is also observed that the heated air surrounding the device forms a hot-air balloon shaped circle reflecting the buoyancy effect of convection.

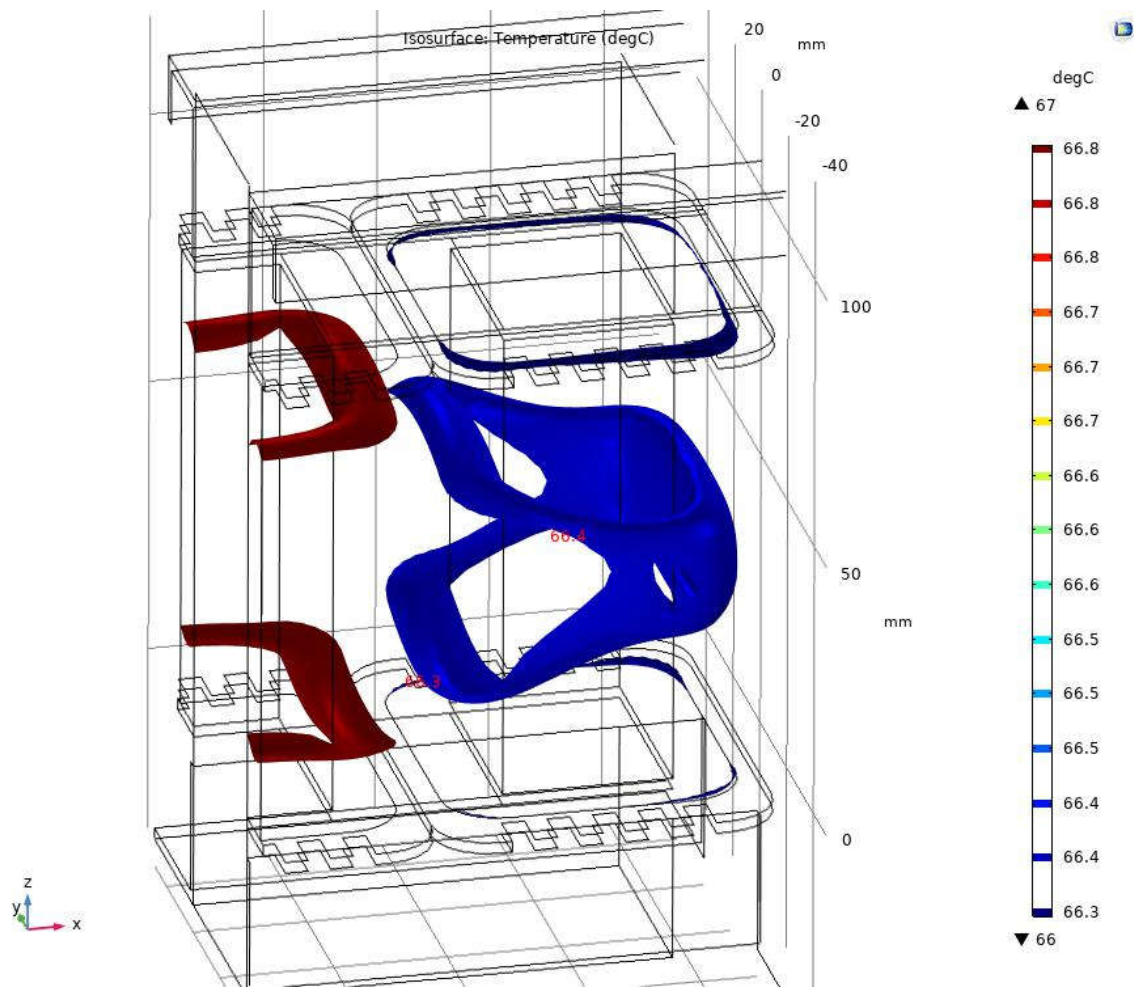


Figure 6.4 Isothermal contour of copper windings

Isothermal contours represent the temperature profile and gradient inside the volume. Although a fixed amount of heat energy is assigned, copper windings display a minor difference in isothermal contours as shown in Figure 6.4. The middle part of the winding shows little higher temperature than the other one on the outside due to the position in the middle where more heats are gathered and transmitted to upside and downside.

Wider contour gap implies more uniform vertical temperature distribution as seen in the middle winding. For the side winding where 2 isothermal contours incline up and down respectively and almost meet at the end, it tells us that the vertical temperature gradient on the side of the winding surface is bigger than others due to more convection to the air taking place at the side.

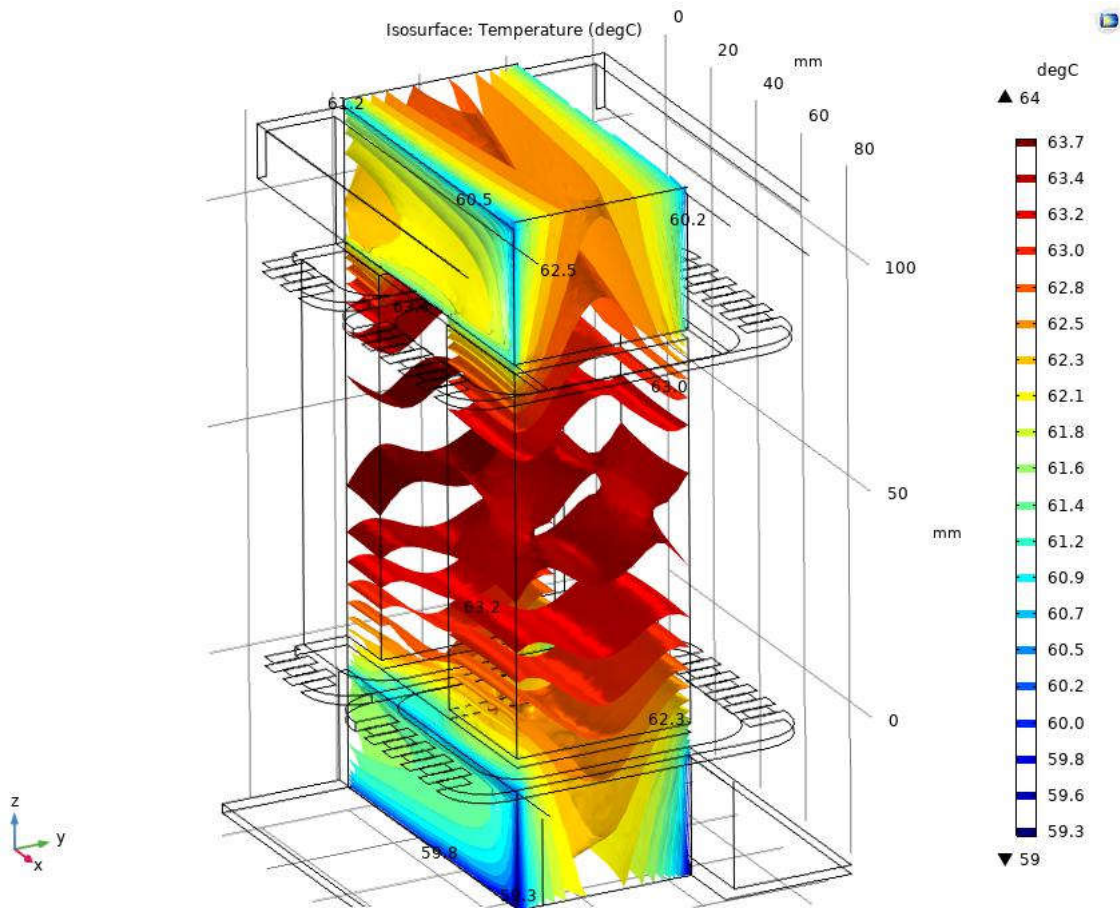


Figure 6.5 Isothermal contour of E-core

Unlike copper windings, the temperature profile inside the transformer core is much more complicated as shown in Figure 6.5. The isothermal contours stay in a form of curved plane layers in the middle of the core leg but tend to bend to form a triangular cone shape as it moves to the top or the bottom. It's because the more vigorous heat conduction takes place at the top and the bottom. At last when in contact with the frame parts, the contour becomes almost vertical sheets. The core part with brown colour contour shows the highest temperature close to 64 °C and the corner vertices in contact with the air and the frame shows the lowest temperature of around 59 °C.

6.2 Heat flux analysis

Heat transfer data together with the temperature is plotted according to the axis and planes. It would be meaningful to speculate the flux and temperature changes along the fixed line on x-axis. As shown in Figure 6.6, the total heat flux magnitude in W/m^2 and temperature along the x-coordinate at $z=85$ mm is retrieved from the simulation results.

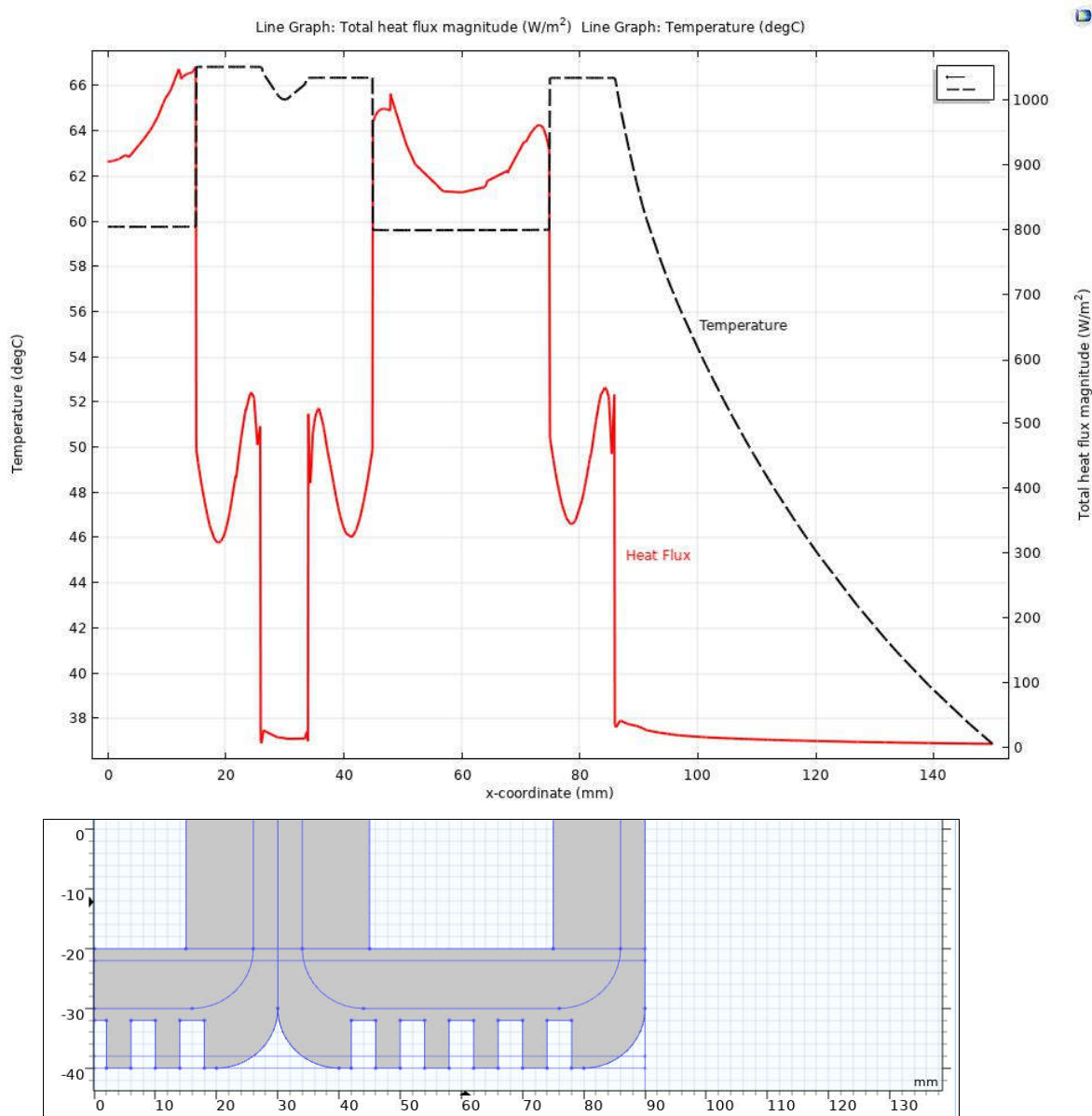


Figure 6.6 Temperature and heat flux magnitude along x-coordinate at $z=85$ mm and the bobbin geometry along the x-axis

The starting point $x=0$ is the middle point of the transformer where axisymmetric coordinate starts. Heat flux is an amount of heat energy projected and flowing through the area, so the value increases at boundary surfaces and decreases in the volume domain. It is observed the flux increases to its maximum value as it approaches $x=15$ where the core and the copper winding meets. These 2 heat sources exchange the biggest amount of heat energy in the model.

It is also confirmed in the model that the surface temperature and the heat flux on the middle winding surface are higher than those on the other winding surfaces. It reflects that radiation between copper winding surfaces and the middle part receiving more heat

flux via convection than the side ones contribute to the temperature rise. The lowest flux is measured around $x=30$ where air passage between windings are placed and the section after $x=85$ where the transformer geometry ends.

Heat flux is a vector quantity and since Figure 6.6 only deals with the magnitude (sum of x , y , and z directions), the heat flux curve does not associate proportionally with the temperature fluctuation. However, heat flux increases where there is a temperature rise or fall and vice versa.

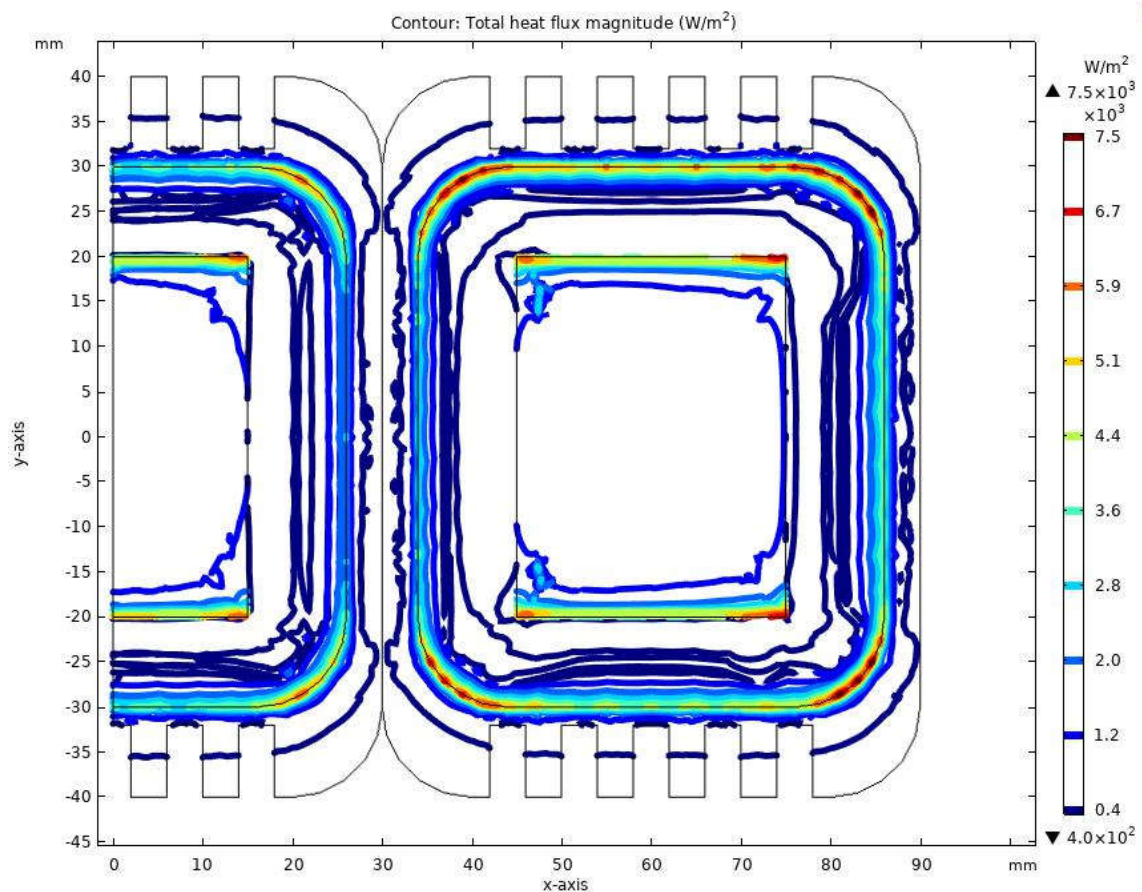


Figure 6.7 Total heat flux contour at the upper bobbin ($z=85$ mm)

As shown in Figure 6.7, the horizontal cross-sectional plane is taken at the upper bobbin area to observe the heat transfer in the section. Filleted corners of the windings display a higher heat transfer rate than the other straight-lined surfaces. A distinctively higher temperature is observed at the upper and the lower horizontal surface lines between the core and the inner winding ($y=20$ and $y=-20$). It's mainly because the edge of the top frame part is in contact with the bobbin along this line resulting in more conductive heat transfer through the straps.

Temperature contour is also taken as shown in Figure 6.8 for a comparison with the heat flux contour.

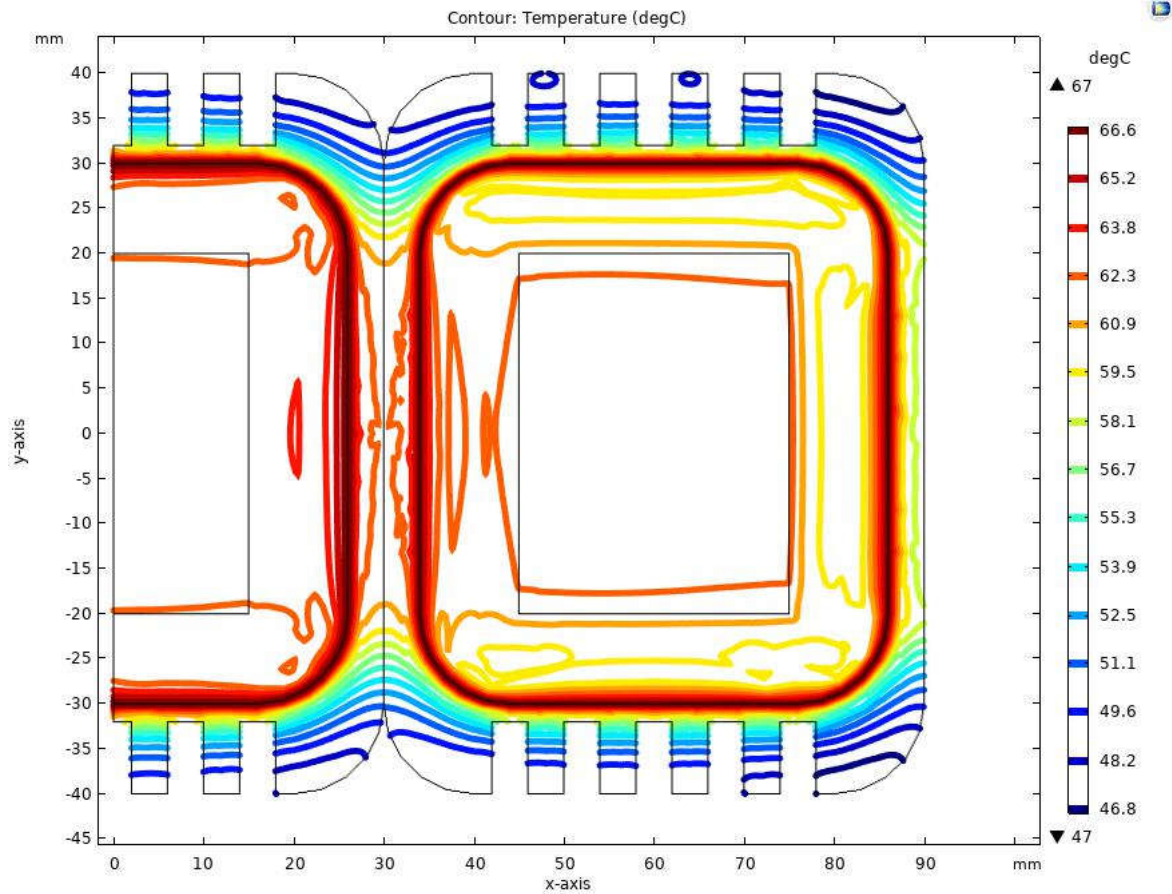


Figure 6.8 Temperature contour at the upper bobbin (x-y plane cut at z=85 mm)

The copper windings and the inner cores display regular temperature distribution with minor irregular contours inside. Brown and red coloured contours which are in contact with the outer winding surface displays the hottest temperature. Not many contours are formed along the inner bobbin due to the thermal equilibrium state already reached which means the temperature of the core leg and the copper windings are almost the same.

Between $x=25$ and $x=35$ where air passage is between windings, temperature contours with some turbulence of hot air are observed caused by convection and radiation. Similar turbulence can be found in heat flux pattern in Figure 6.7.

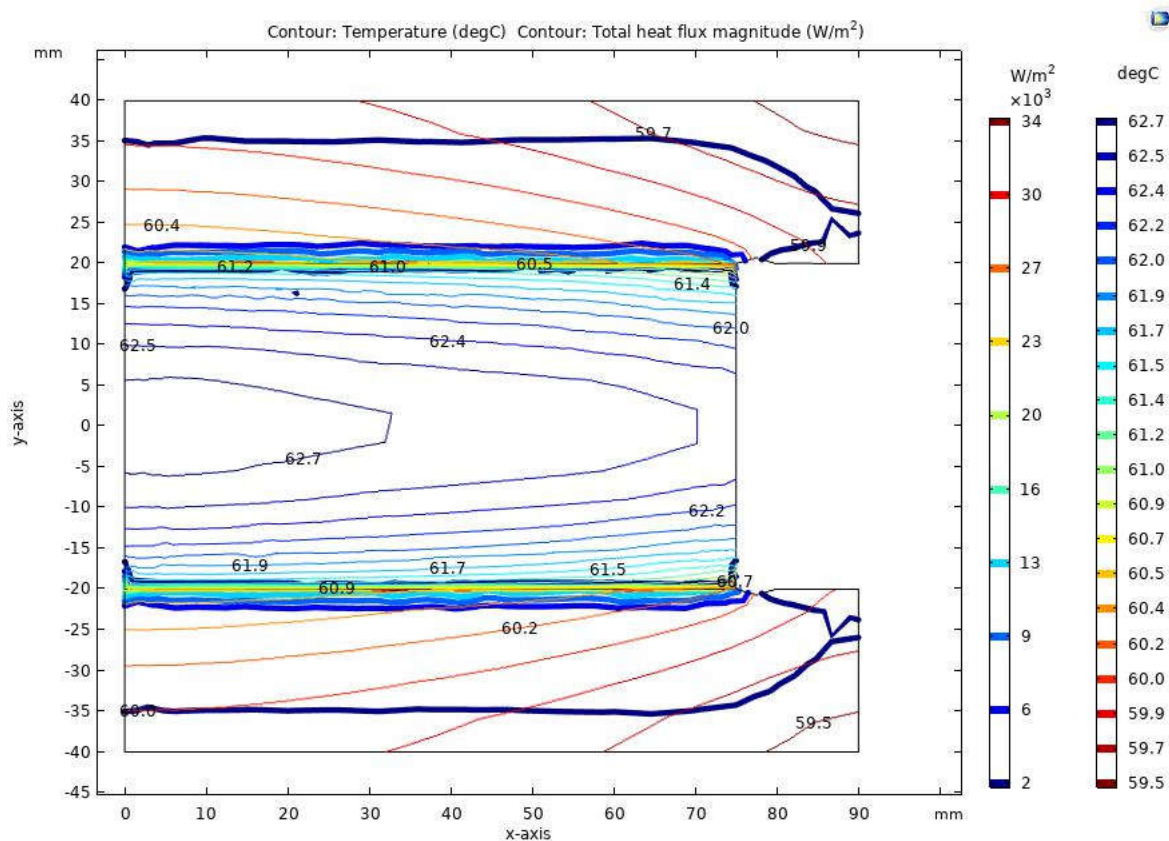


Figure 6.9 Heat flux and temperature contour of the top frame at $z=117$ mm

Heat flux and temperature contour of the top frame is displayed together in Figure 6.9. The hottest temperature contour is formed in the middle of the top core with a temperature of $62,7$ °C. Isothermal contours are formed almost horizontally on the top core due to the anisotropic conduction characteristic. On the contrary to this, temperature contours on the top frame demonstrate isotropically but inclined to the right end. It tells us that the right end of the frame is more cooled conducting more heats to this direction resulting in such bending of the contours.

When it comes to heat energy transfer, most vigorous heat flux is taking place at $y=20$ and $y=-20$ where 3 domains, air, top frames, and E-core meet together. The average values of temperature and total heat flux magnitude according to the domains and boundaries are presented in Table 6.2.

Table 6.2 Average temperature and heat flux values over boundary and domain

Surface Boundary	Winding	E-Core	Inner Bobbin
Average Temperature	66.9 °C	61.4 °C	65.0 °C
Total heat flux magnitude (W/m^2)	282.9	1757.4	602.8

Normal conductive heat flux (W/m ²)	179.9	307.6	-184.0
Radiative heat flux (W/m ²)	8.0	5.1	6.1

Volume (Domain)	Winding	E-Core	Frame	Bobbin
Average temperature	66.9 °C	62.7 °C	59.8 °C	58.4 °C
Total heat flux magnitude (W/m ²)	329.1	600.8	2358.2	328.1

Observing the average total heat flux, winding has shown the least and the E-core the most. Again, heat flux being a vector quantity, they cancel out if they exchange heat transfer, thus winding part is actively involved in exchanging heat with the E-core. Interestingly, normal conductive heat flux of the inner bobbin boundary shows a negative value which means that there is more inward flux from the windings than the outward flux from the E-core. Total heat flux by the volume domain tells us that the most heats are dissipated to the air through the frame.

6.3 Airflow analysis

The flow of the air around the transformer should be analysed for convection plays an important role in cooling. Setting and adjusting the size of the air domain is a tricky task that requires many trial and error. Air domain should be big enough not to affect the convective cooling but small enough not to waste computational resources. As shown at time=0 min. in Figure 6.10, two red marks on both corners of the air domain has meaningless velocity flow came from the difference between the reference temperature usually set as 193,15 K and the ambient air temperature set as 23 °C.

Furthermore, when time=0, the velocity of air shows the almost symmetrical distribution. However, the velocity of the whole air domain is not uniform. It comes from the structure of the model that heat sources are directly applied to the volume causing the existence of the heat even at the beginning. Unfortunately, the heat sources are not able to be controlled by any initial conditions, thus, non-zero and non-uniform air velocity is observed at time=0.

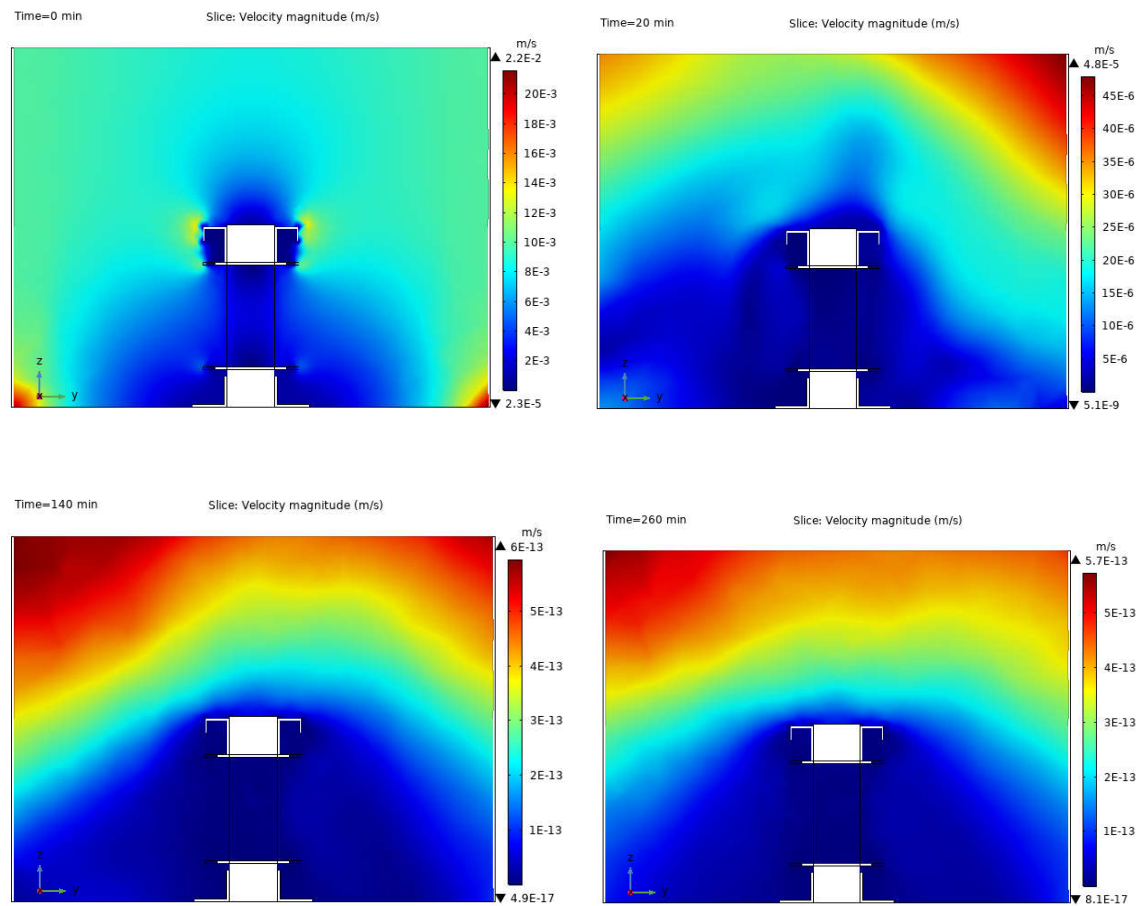


Figure 6.10 Velocity field on YZ plane at $x=30\text{mm}$ (Time=0, 20, 120, 260 min.)

Nevertheless, as time goes on, velocity field changes with irregular gradient due to the change in air density associated with the turbulence. When the air is fully heated around the device, the density changes less and the air velocity drops accordingly.

Another important perspective in convection is the diffusivity of the flow and this can be intuitively studied by observing Prandtl number (Pr) mentioned previously. Higher the Pr means slow in diffusivity and the smaller the Pr , the faster the diffusivity. In general, Pr value of gases lies between 0,7 and 1,0, and water between 1,7 and 13,7 [19].

As shown in Figure 6.11, Pr value around the device is over 1,4 which shows low diffusivity but Pr drops as time goes by and reaches below 1 at 260 min. Based on the definition, the drop of Pr tells us that the heat diffusivity gets bigger than the momentum diffusivity.

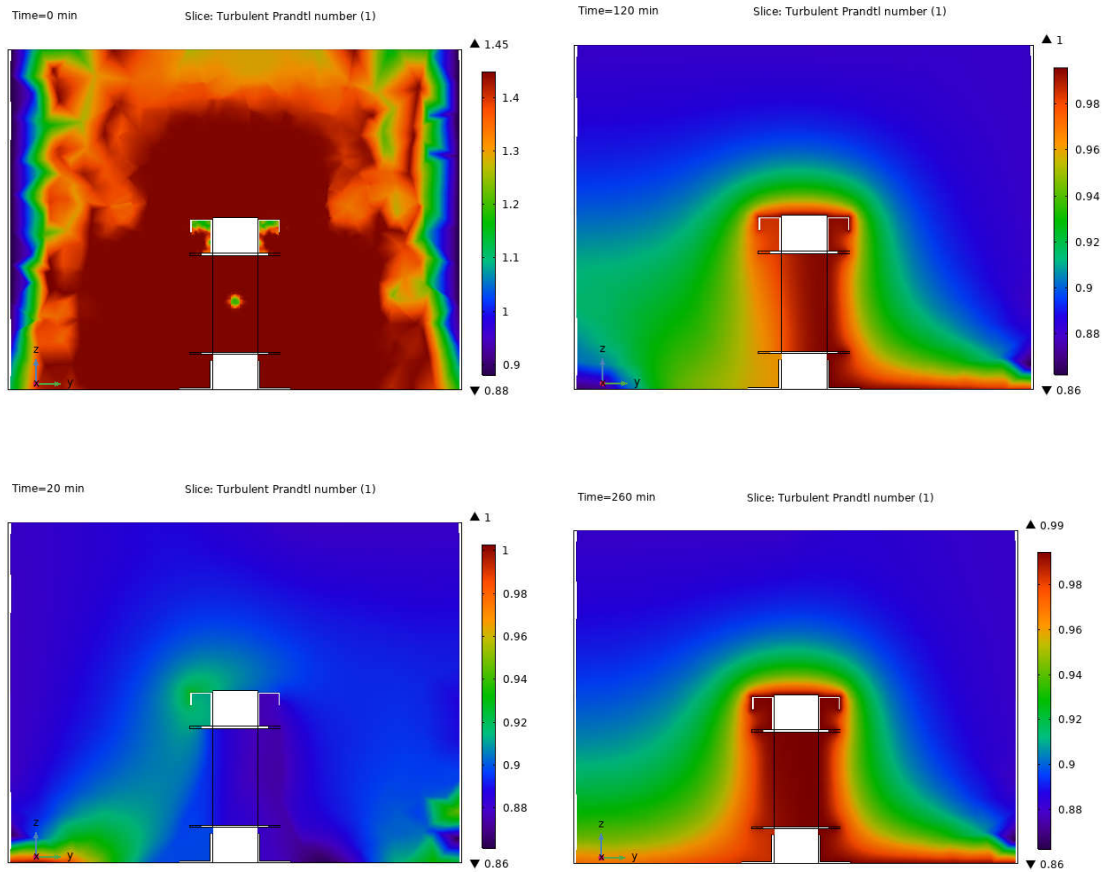


Figure 6.11 Diffusivity on YZ plane at x=30 mm (Time=0, 20, 120, 260 min.)

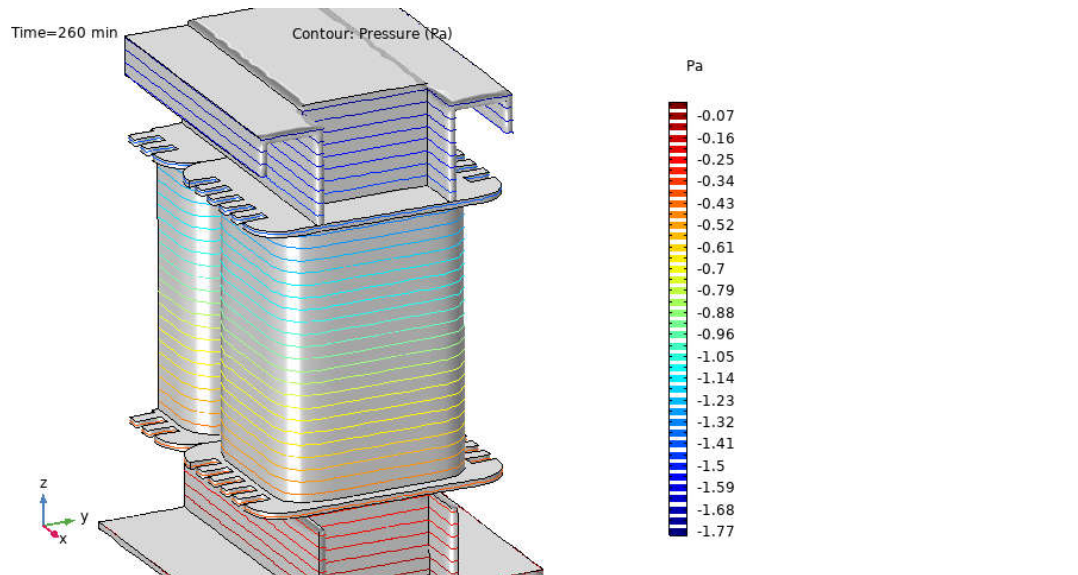


Figure 6.12 Pressure contour around the transformer surface at time=260 min.

Relative pressure difference caused by the heated air is demonstrated in Figure 6.12. There is a pressure difference of about 1,7 Pa along with the height of the transformer

and this pressure difference causes buoyancy force leading convection along the surface wall of the device.

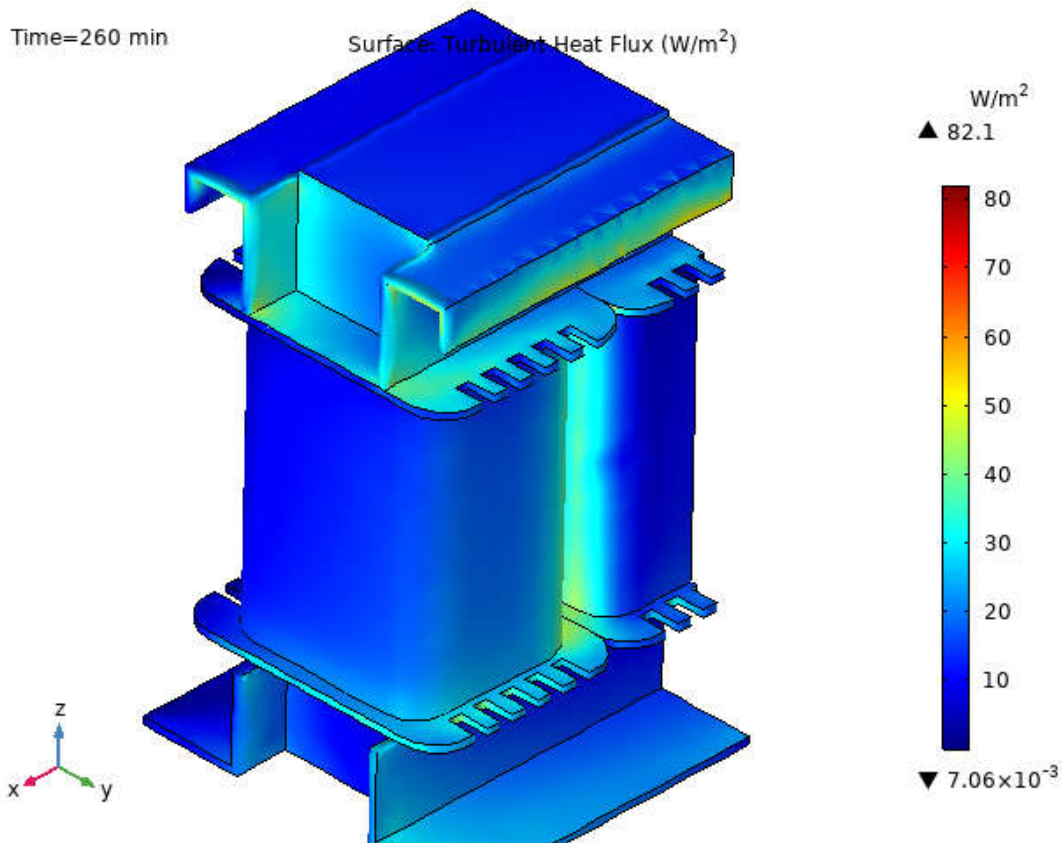


Figure 6.13 Turbulent heat flux over the surface at time=260 min.

Turbulent heat flux over the device surface is depicted in Figure 6.13. This can be referred to as convective heat transfer from the surface to the ambient air caused by turbulent airflow. Nevertheless, certain circulation of airflow inside the air domain is observed that is considered abnormal and this would somehow affect the cooling effect of the device. Therefore, more intensive study and remodelling of the air domain should be carried out to accurately calculate and extract the heat transfer coefficients for convection and radiation over the surface.

6.4 Conclusion and discussion

The main aim of the research is achieved by approximating the surface temperature of the simulation to that of the experiment. Comparison of surface temperatures gained from the experiment and the simulation is shown in Table 6.3.

Table 6.3 Temperature comparison between the experiment and the simulation

	Copper windings		E-Core top	Top Frame	Foot frame
	Average	Hottest	Average	Average	Average
Experiment	64,1 °C	74,2 °C	54,1 °C	59,8 °C	61,9 °C
Simulation	66,9 °C	67,3 °C	61,4 °C	60,3 °C	59,7 °C
Difference	2,8 °C	6,9 °C	7,3 °C	0,5 °C	2,2 °C

Although the highest average temperature achieved from the simulation is lower than the hottest temperature measured from the experiment, the average temperature from the simulation lies between the hot spot temperature and the average temperature measured from the experiment. The temperature gradient in the real copper windings is much wider-ranging from minimum 57,4 °C to maximum 74,2 °C. The temperature difference of 16,8 °C is not a small scale and it shows a non-linear pattern over the surface whereas the copper windings in the simulation model show almost identical temperature distribution over the entire domain.

In this regard, there are crucial limitations on this study which does not provide analytical information on the heat sources, especially the copper windings where the hottest temperature is detected. It comes from the hypothesis of the study that heat sources are not modelled but rather experimentally obtained values are directly assigned to the copper windings and E-core domains.

Air is actually enclosed in the winding, thus both conduction and convection take place inside the winding domains. Since it is not practical to fully model this, only conduction is considered resulting uniform surface temperature. The hot air inside the windings and the irregular winding tensions could explain the appearance of hot spots. Therefore, a separate electro-magnetism model which includes winding geometry and air can be modelled in the future based on Joule heating model to achieve more realistic study results on the winding.

E-core temperature shows the biggest difference. It is probably due to the inaccuracy of the temperature measurement and the anisotropic heat transfer coefficient used in

the simulation which is taken from the other manufacturer's specification.

Measurement area taken from the thermal image for the E-core top was limited due to the focus issue and the wires interference. More thermocouples in different locations could improve such deviations.

The temperature of E-core is higher than the frame temperature in simulation, whereas E-core temperature is lower than the frame temperature. As E-core acts as the second hot source also receiving additional heat from the windings, it is logic that E-core should have a higher temperature than the frame. However, the experiment result demonstrates the opposite. It implies that heats from the copper windings are being transferred upward to the frame by convection and radiation heating up the frame more than the E-core.

The foot frame temperature is discovered to be much higher than that of the upper frame temperature. Supposed that the materials and the heat transfer rates are same, the upper part should be exposed to more heat flux due to the buoyancy convection. The main cause would be geometry and position. The contact between the foot frame and the floor is not uniform, however, it definitely hinders heat being dissipated to the air.

Considering there is no forced convection, conduction affects far more than natural convection on frame parts. Steel frames are acting as fins to cool down the device especially at the upper part of the frame. It could be concluded that well-designed frame parts with good quality materials can cool down the transformer considerably.

There were some obstacles while carrying the experiment. The thermal image resolution was not high enough and obtaining the well-focused image was not easy. It would have been better if the camera could be fixed on a tripod. Also, some important technical information such as the number of turns was not available from the manufacturer. It was based on the specification from a similar transformer and number of turns and the copper wire thickness are adjusted to satisfy the copper loss value obtained from the experiment.

Future work can be discussed in connection with the study as follows.

In Comsol, electromagnetism study can be utilized. A separate model, especially on the copper windings, can be created to apply the Joule heating model of the CFD tool to simulate copper losses. This can be approached by using current flux density through the vertical cross-sectional area of the winding part. In this way, a detailed

single wire does not have to be modelled but numerical coils can be defined with current flux through the cross-sectional area. Nevertheless, Comsol does not provide a means to model and calculate iron losses directly from the electromagnetism model. It requires numerical post-processing using other software such as Matlab. This is another area to research.

SUMMARY

Thermal analysis model of a 3 phase power transformer is modelled in an axisymmetric geometry. No-load test and the open-circuit test is carried to find out the exact values of copper losses and iron losses. The fully loaded test is carried out to measure the surface temperature of the transformer for 240 min. Simulation of the transformer is performed using numerical thermal analysis. The simulation result shows the agreeable result in comparison with the experiment result.

Temperature distribution over the copper winding surface shows the almost uniform temperature whereas experimental result demonstrates deviation and irregular distribution. Frame parts of the transformer play a great role in cooling the device. The lower parts of the device, such as foot frame part and the lower side of the core, show relatively higher temperature than the upper parts of the device.

[Kokkuvõte]

Kolmefaasilise toitetrafo termilise analüüsi mudel on modelleeritud telgsümmeetrilises geomeetrias. Vasekao ja rauakao täpsete väärtuste väljaselgitamiseks viiakse läbi koormustesti ja avatud voluringi katse. Trafo pinnatemperatuuri mõõtmiseks 240 min jooksul viiakse läbi täislastis test. Trafo simuleerimine toimub numbrilise termilise analüüsi abil. Simulatsiooni tulemus näitab testi tulemusega võrreldes rahuldavat tulemust.

Temperatuuri jaotus vaskmähise pinna kohal näitab peaaegu ühtlast temperatuuri, eksperimentaalne tulemus näitab kõrvalekallet ja ebakorrapärast jaotust. Trafo raamiosad mängivad seadme jahutamisel suurt rolli. Seadme alumised osad, nagu näiteks jalaraami osa ja südamikü alumine kül, näitavad suhteliselt kõrgemat temperatuuri kui seadme ülemised osad.

LIST OF REFERENCES

- [1] J. Reinert, A. Brockmeyer, and R. W. A. A. De Doncker, "Calculation of losses in ferro- and ferrimagnetic materials based on the modified Steinmetz equation," *IEEE Trans. Ind. Appl.*, vol. 37, no. 4, pp. 1055–1061, Jul. 2001.
- [2] K. Venkatachalam *et al.*, "Accurate Prediction of Ferrite Core Loss with Nonsinusoidal Waveforms Using Only Steinmetz Parameters," 2002.
- [3] T. A. Saandy, M. Rakotomalala, S. Mze, A. F. Toro, and A. Jaomiary, "Analytical Determining Of The Steinmetz Equivalent Diagram Elements Of Single-Phase Transformer," *Int. J. Sci. Technol. Res.*, vol. 4, 2015.
- [4] L. Havez, E. Sarraute, and Y. Lefevre, "3D Power Inductor: Calculation of Iron Core Losses."
- [5] S. H. Westad, "Loss Analysis in Laminated Iron Cores using COMSOL Multiphysics and LiveLink for Matlab Sondre Hamarheim Westad," no. June, 2018.
- [6] Giorgio Bertotti, "General properties of power losses in soft ferromagnetic materials," *IEEE Transactions on Magnetics*, vol. 24, no. 1. pp. 621–630, 1988.
- [7] J. Gastelurrutia, J. C. Ramos, G. S. Larraona, A. Rivas, J. Izagirre, and L. Del Río, "Numerical modelling of natural convection of oil inside distribution transformers," *Appl. Therm. Eng.*, 2011.
- [8] F. Torriano, M. Chaaban, and P. Picher, "Numerical study of parameters affecting the temperature distribution in a disc-type transformer winding," *Appl. Therm. Eng.*, 2010.
- [9] P. E. Blanco Alonso, A. Meana-Fernández, and J. M. Fernández Oro, "Thermal response and failure mode evaluation of a dry-type transformer," *Appl. Therm. Eng.*, vol. 120, pp. 763–771, 2017.
- [10] N. El Wakil, N. C. Chereches, and J. Padet, "Numerical study of heat transfer and fluid flow in a power transformer" A preliminary version of the paper was presented at CHT-4: An ICHMT International Symposium on Advances in Computational Heat Transfer, April 2004, G. de Vahl Davis and E. Leonardi (Eds.), CD-RDM Proceedings, ISBN 1-5670-174-2, Begell House, New York, 2004., " *Int. J. Therm. Sci.*, vol. 45, no. 6, pp. 615–626, Jun. 2006.
- [11] M. Lee, H. A. Abdullah, J. C. Jofriet, D. Patel, and M. Fahrioglu, "Air temperature effect on thermal models for ventilated dry-type transformers," *Electr. Power Syst. Res.*, vol. 81, no. 3, pp. 783–789, 2011.
- [12] Marvin Gerth, *Transformers for the Electrician*. 2009.
- [13] J. H. Harlow, *Electric Power Transformer Engineering*, 3rd ed. CRC Press, 2012.
- [14] Electronic Tutorials, "Three Phase Transformer Connections and Basics."

- [Online]. Available: <https://www.electronics-tutorials.ws/transformer/three-phase-transformer.html>. [Accessed: 02-Dec-2019].
- [15] All about circuit, "Three-phase Transformer Circuits | Polyphase AC Circuits | Electronics Textbook." [Online]. Available: <https://www.allaboutcircuits.com/textbook/alternating-current/chpt-10/three-phase-transformer-circuits/>. [Accessed: 21-Nov-2019].
- [16] Robert W. Erickson, *Fundamentals of Power Electronics 2nd Edition*, 2nd edition, no. February. Kluwer Academic Publishers, 2004.
- [17] V. H. Juha Pyrhonen, Tapani Jokinen, "Design of Rotating Electrical Machines," John Wiley & Sons, Ltd, 2008, pp. 457–460.
- [18] P. Goes and M. De Wulf, "Calculating Iron Losses Taking into Account Effects of Manufacturing Processes," *Comsol Conf. Hann. 2008*, vol. 2, 2008.
- [19] Y. A. C. A. J. Ghajar, *Heat and Mass Transfer - Fundamentals & Applications*. 2011.
- [20] G. F. Naterer, *Advanced Heat Transfer*, Second edition, vol. 53, no. 9. CRC Press, 2018.
- [21] "Two Wattmeter Method of Power Measurement - In Star & Delta Connection-Circuit Globe." [Online]. Available: <https://circuitglobe.com/two-wattmeter-method-of-power-measurement.html>. [Accessed: 14-Dec-2019].
- [22] Flir, "User's manual: FLIR Exx series," 2010, p. 206, 2010.
- [23] "Infrared Camera Accuracy and Uncertainty in Plain Language | FLIR Systems." [Online]. Available: <https://www.flir.com/discover/rd-science/infrared-camera-accuracy-and-uncertainty-in-plain-language/>. [Accessed: 01-Jan-2020].
- [24] Thorwald L. van Vuure, "Anisotropic Heat Transfer in Orthocyclically Wound Coils," *Proc. 2013 Comsol Rotterdam*, 2013.
- [25] CogenPower, "Electrical steel property," p. 3.
- [26] I. R. A. A. Mousawi Dr. Abdul Jabbar N. Khalif, "Comparison of Heat Transfer Coefficients in Free and Forced Convection using Circular Annular Finned Tubes," *IJAIEEM*, vol. 5, no. 4, p. 203, 2016.
- [27] "How to Inspect Your Mesh in COMSOL Multiphysics® | COMSOL Blog." [Online]. Available: <https://www.comsol.com/blogs/how-to-inspect-your-mesh-in-comsol-multiphysics/>. [Accessed: 30-Dec-2019].

APPENDICES

Name	Expression	Value	Description
coreW	150 [mm]	0.15 m	Core top width
coreH	152 [mm]	0.152 m	Core top height
coreD	40 [mm]	0.04 m	Core top depth
corelegW	30 [mm]	0.03 m	Ecore leg width
corelegD	windD-windT*2	0.04 m	Ecore leg depth
windW	52 [mm]	0.052 m	Copper winding width
windD	60 [mm]	0.06 m	Copper winding depth
windH	85 [mm]	0.085 m	Copper winding height
windT	10 [mm]	0.01 m	Copper winding thickness
teethW	4 [mm]	0.004 m	Bobbin teeth width
teethD	10 [mm]	0.01 m	Bobbin teeth depth
teethT	2 [mm]	0.002 m	Bobbin teeth thickness
gap	$(\text{coreW} - (3 * \text{corelegW})) / 2$	0.03 m	Gap between cores
AirD	300 [mm]	0.3 m	air domain diameter
AirH	350 [mm]	0.35 m	air domain height

Figure A.0.1 Geometric parameters in Comsol

Table A.1 Detailed temperature measurement data of the experiment

Time (min.)	Thermo couple ①	Thermal Img.Spt ②	Windings					① - ②
			A	B	C	Average	Hot Spot	
0	24,1 °C	24,1 °C	24,0 °C	24,1 °C	24,0 °C	24,0 °C	24,1 °C	0
20	38,9 °C	38,9 °C	40,4 °C	40,5 °C	41,1 °C	40,7 °C	45,0 °C	0
40	45,5 °C	45,1 °C	47,3 °C	47,3 °C	47,8 °C	47,5 °C	53,5 °C	0,4
60	48,7 °C	48,9 °C	51,9 °C	51,5 °C	52,3 °C	51,9 °C	59,2 °C	0,2
80	51,6 °C	51,7 °C	55,2 °C	54,2 °C	55,7 °C	55,0 °C	63,2 °C	0,1
100	53,4 °C	53,9 °C	57,6 °C	56,7 °C	57,9 °C	57,4 °C	66,6 °C	0,5
120	54,8 °C	54,2 °C	59,4 °C	58,3 °C	59,4 °C	59,0 °C	68,5 °C	0,6
140	55,9 °C	55,9 °C	60,7 °C	59,3 °C	61,0 °C	60,3 °C	69,9 °C	0
160	57,1 °C	56,4 °C	61,7 °C	60,0 °C	61,9 °C	61,2 °C	71,4 °C	0,7
180	57,8 °C	57,3 °C	62,5 °C	60,9 °C	62,6 °C	62,0 °C	72,3 °C	0,5
200	58,3 °C	58,1 °C	63,1 °C	61,6 °C	63,6 °C	62,8 °C	72,5 °C	0,2
220	58,8 °C	58,8 °C	64,1 °C	62,5 °C	64,0 °C	63,5 °C	74,4 °C	0
240	59,2 °C	58,7 °C	63,9 °C	62,6 °C	63,7 °C	63,4 °C	74,0 °C	0,5
260	59,2 °C	58,8 °C	64,1 °C	62,8 °C	64,1 °C	63,7 °C	74,2 °C	0,4
							Average:	0,3 °C

Table A.1 (Continued) Detailed temperature measurement data of the experiment

Time (min.)	Ecore			Frame				
	Top	SideTop	Side Bott.	FR_top	FR_Bott.	Foot	Top	
0	24,5 °C	24,0 °C	24,2 °C	24,0 °C	24,2 °C	24,3 °C	24,2 °C	
20	30,1 °C	31,3 °C	28,8 °C	31,3 °C	28,8 °C	31,0 °C	32,3 °C	
40	36,3 °C	33,0 °C	36,5 °C	37,5 °C	35,1 °C	39,4 °C	40,5 °C	
60	41,4 °C	36,0 °C	41,1 °C	42,3 °C	39,5 °C	45,3 °C	45,3 °C	
80	45,2 °C	38,0 °C	45,3 °C	45,4 °C	43,0 °C	49,1 °C	49,6 °C	
100	47,3 °C	40,2 °C	47,7 °C	48,2 °C	45,3 °C	53,4 °C	53,3 °C	
120	49,2 °C	40,5 °C	49,8 °C	49,7 °C	47,0 °C	55,7 °C	54,8 °C	
140	50,8 °C	41,3 °C	51,0 °C	50,8 °C	48,8 °C	57,5 °C	56,1 °C	
160	52,0 °C	42,5 °C	52,1 °C	51,6 °C	49,6 °C	58,6 °C	57,3 °C	
180	52,5 °C	43,0 °C	53,1 °C	52,6 °C	50,6 °C	59,5 °C	58,2 °C	
200	52,9 °C	43,4 °C	53,8 °C	53,4 °C	51,2 °C	60,5 °C	59,2 °C	
220	53,7 °C	43,4 °C	54,0 °C	53,7 °C	52,6 °C	61,2 °C	60,0 °C	
240	53,9 °C	43,3 °C	54,4 °C	54,1 °C	52,0 °C	62,6 °C	60,5 °C	
260	54,1 °C	43,7 °C	54,3 °C	54,2 °C	52,2 °C	61,9 °C	59,8 °C	

Table A.2 Materials and thermal properties of each surface and domain

		E-Core		Copper	
		Surface	Domain	Surface	Domain
Material		Si Steel (3%)		Cellulose	Copper
Thermal Conductivity, k	W/m·K	28	28	k(T)	400
Surface Emissivity, ϵ	-	0,8	-	0,9	0,5
Specific Heat, C_p		600	600	2000	385
Density, ρ	Kg/m ³	7650	7650	51	8940

		Frame surface		Frame Domain	Bobbin	Floor
		Top	Foot			
Material		iron	enamel	iron	Zenite	plaster
Thermal Conductivity, k	K	76,2	0,93	76,2	0,32	0,24
Surface Emissivity, ϵ	-	0,25	0,37	-	0,95	0,91
Specific Heat, C_p		440	715	440	125	-
Density, ρ	Kg/m ³	7870	2800	7870	1620	-